Consistent Evaluation of the Prompt-fission Neutron Spectrum and Multiplicity for n+^{235,238}U and n+^{239}Pu

A.E. Lovell, D. Neudecker, P. Talou, I. Stetcu, M.J. Grosskopf, T. Kawano
Los Alamos National Laboratory, Los Alamos, NM, 87545, USA

September 18, 2020

Contents

Abstract

This report was written to satisfy a FY20 NCSP milestone on ^{235,238}U and ^{239}Pu. The milestone requires to "finalize a report assessing our methodology to evaluate prompt-fission neutron spectrum (PFNS) and multiplicity consistently". More specifically, we study whether the code `CGMF` can reproduce ENDF/B-VIII.0 evaluated PFNS and average prompt-fission neutron multiplicities, $\overline{\nu}$, for ^{235,238}U and ^{239}Pu using one joint parameter set per isotope. If `CGMF` is shown to be able to reasonably reproduce ENDF/B-VIII.0 within its model-parameter space, this code could be used for future consistent evaluations of PFNS and $\overline{\nu}$. To answer this question, we explore here the parameter space of `CGMF` and its impact on calculated values and whether they are close to evaluated and experimental data. We also list experimental data that would enter a future evaluation and statistics method that could be used to obtain evaluated data and covariances. We conclude that values of $\overline{\nu}$ calculated by `CGMF` are reasonably close to ENDF/B-VIII.0 data, while more work on modeling the PFNS is needed (parameter optimization and model improvements) to reliably use it for evaluations.

Keywords: Average Prompt-fission Neutron Multiplicity, Prompt-fission Neutron Spectrum, ^{239}Pu, ^{235}U, ^{238}U, CGMF

LA-UR-20-26932

1 Introduction

This report is in answer to the FY20 NCSP milestone on ^{235,238}U and ^{239}Pu that requires to "finalize a report assessing our methodology to evaluate PFNS (Prompt-fission Neutron Spectrum) and multiplicity consistently". The goal is to use the `CGMF` code [1, 2] to model the PFNS and the average prompt-fission neutron multiplicity, $\overline{\nu}$. Even more specifically, the aim is to investigate whether one can match ENDF/B-VIII.0 PFNS and $\overline{\nu}$ nuclear data [3] within the parameter space of the CGMF framework while taking into account auxiliary data for the modeling and comparing to other output data. One of these possible outputs of `CGMF`, that can be counter-checked against experimental data, is, *e.g.*, the angular distributions of neutrons or prompt-fission gamma spectra. The reason for this undertaking is to explore whether `CGMF` could be used in the future to produce consistently evaluated PFNS and $\overline{\nu}$ for the same isotope.

The `CGMF` code is a Monte Carlo implementation of the Hauser-Feshbach statistical theory of nuclear reactions, applied to the de-excitation of the scission fragments through the evaporation of prompt neutrons and γ rays. As input, it requires the pre-neutron-emission fission-fragment yields in mass, charge and total kinetic energy, $Y(A, Z,\text{TKE})$. As output, it provides an event-by-event record of fission decays that contains the initial fission-fragment conditions, including its initial momentum vector, and all characteristics (multiplicity, energies, momenta) of all accompanying emitted particles (neutrons and γ rays). Average quantities, distributions (energy, angle), and correlations among all those particles and the fragment they originate from can all be obtained through straightforward accounting and statistical techniques.

Two of those average quantities are particularly interesting in view of data present in the ENDF/B-VIII.0 library: the PFNS and $\overline{\nu}$. In ENDF/B-VIII.0, these two quantities are given for incident-neutron energies from thermal up to 20 MeV. The PFNS for both n+^{235}U and n+^{239}Pu were recently revisited [4] in light of experimental data from Chi-Nu [5]. The ^{235}U(n,f) $\overline{\nu}$ was modified to include fluctuations near the thermal point due to the (n,γf) process. The average neutron multiplicity for ^{239}Pu was slightly modified in the fast region to account for integral-benchmark feedback, including sub-critical experiments. No consistency between PFNS and $\overline{\nu}$ was considered in the evaluation process.

However, the `CGMF` code can be used to produce consistent calculations of PFNS and $\overline{\nu}$, as a function of incident-neutron energy, from thermal up to 20 MeV. The input fission-fragment yields, $Y(A, Z, \text{TKE}|E_{\text{inc}})$, have been derived and implemented in `CGMF` already. Other model input parameters, primarily the $\langle\text{TKE}\rangle$ values, have been adjusted to reproduce $\overline{\nu}$ across the incident-energy range.

Due to these adjustments of model parameters, the calculated $\overline{\nu}$ values for ^{235,238}U and ^{239}Pu are shown to be reasonably close to ENDF/B-VIII.0 in Section 5. Some systematic deviations of calculated data from evaluated data are observed at second-chance fission pointing to shortcomings in fission-probability parameters and maybe the incident-neutron energy dependence of $\langle\text{TKE}\rangle$. For $\overline{\nu}$, we expect that one can produce realistic evaluated data with `CGMF` when optimizing the model parameters to experimental data.

The `CGMF` PFNS, however, has always been calculated too soft compared to measured data; and that is the case here for all three isotopes studied with the initial parameters of `CGMF` tweaked to get good agreement to $\overline{\nu}$. But the PFNS's systematic behavior is different across isotope: ^{238}U PFNS, while still too soft, are closest to experimental data below second-chance fission, while ^{235}U and ^{239}Pu PFNS are clearly far away from experimental data. Also, all PFNS suffer from obvious issues at second-chance fission pointing again to the need for optimizing the fission-probability, *etc.*, parameters. The shape of the average outgoing-neutron energy or mean energy of the ^{239}Pu PFNS, *i.e.*, the first moment of the spectrum, as a function of incident-neutron energy has been shown to be in reasonable agreement with the Chi-Nu data for ^{239}Pu except for a systematic, but very significant for applications (up to 100 keV!), off-set. However, this systematic behavior does not apply to ^{235,238}U PFNS mean energies. Hence, the initial parameters set of `CGMF` used here in Section 5 was clearly not satisfactory in reproducing ENDF/B-VIII.0.

Hence, parameter studies were undertaken here to map out in how far one can give more reasonable PFNS while maintaining good agreement for $\overline{\nu}$. Also, this issue was studied by Lovell, Stetcu *et al.* over the summer with students (T.S. Blade and S.D. Ozier) from the "2020 XCP Computational Physics Summer Workshop" using an emulator with discrepancies and is summarized here briefly; this issue was also previously studied by Lovell, Stetcu, Talou, *et al.* during the "2019 XCP Computational Physics Summer Workshop" with students (C. Parker and S. Pineda) to understand the effects of assuming different optical potentials on the PFNS. The information from all these studies is combined here to assess whether we will be able to reproduce ENDF/B-VIII.0 PFNS and what developments need to be undertaken in the future to use `CGMF` for consistent evaluations of PFNS and $\overline{\nu}$.

To study this, we:

1. Perform `CGMF` calculations with default input parameters as described in Section 2. We will also explore to which model parameters the PFNS and $\overline{\nu}$ are sensitive to, and whether optimizations in the parameter space have the potential to improve the agreement of the PFNS with experimental data, shown in Section 3.

2. Collect the most recent PFNS and $\overline{\nu}$ evaluated data and show them in Section 5 in comparison to `CGMF` calculated values and experimental data. The latter are listed in Section 4.

3. Explore in Section 6 which evaluation techniques (Kalman filter, GLS) lend themselves to optimize the `CGMF` input parameters to reproduce the evaluated $\overline{\nu}$ and PFNS as well as yield evaluated covariances for both observables. We will also explore whether emulators paired with Gaussian processes can be used to reliably correct for remaining issues in the PFNS that cannot be resolved by improving the model parameters or the model itself.

A summary of the main findings and a conclusion whether a consistent evaluation of PFNS and $\overline{\nu}$ for one isotope is attainable with `CGMF` is given in Section 7.

2 Overview of the `CGMF` Model

There are several models and data needed for a complete `CGMF` calculation. The multi-chance fission probabilities are an input at each incident-neutron energy and are sampled for each fission event; the fission probabilities for ^{235}U, ^{238}U, and ^{239}Pu are shown in Fig. 1. If one of the multi-chance fission channels, above first chance, is sampled, one or more neutron are emitted from the compound nucleus before fission occurs. Most of these pre-fission neutrons are evaporated from the compound nucleus, and their energy is sampled from an evaporation spectrum. At high enough incident energies, above ~ 12 MeV, the first neutron emitted from, *e.g.*, ^{240}Pu, can be a pre-equilibrium neutron. These neutrons have an energy spectrum and angular distribution more akin to inelastically scattered neutrons. If this channel is energetically available, the first pre-fission neutron out is determined to be a pre-equilibrium neutron or not based on the pre-equilibrium fraction, as shown in Fig. 2. The fraction of pre-equilibrium neutrons is fit, based on calculations from `CoH`$_3$, to the functional form

$$f_{pe} = \frac{1}{1+\exp[(a_0 - E_{\text{inc}})/E_0]} + sE_{\text{inc}} + f_0, \tag{1}$$

where a_0, E_0, s, and f_0 are all fitted parameters and E_{inc} is the energy of the incident neutron. Although the pre-equilibrium fraction is non-zero starting around $E_{\text{inc}} \sim 1.5$ MeV, it is not until $E_{\text{inc}} \sim 12$ MeV that a pre-equilibrium neutron can be emitted from the compound nucleus and leave the resulting nucleus with enough excitation energy to fission. The four fitted parameters for f_{pe} are given in Table I for ^{235}U, ^{238}U, and ^{239}Pu.

To initialize each `CGMF` fission event, a model for the initial conditions of the fission fragments, $Y(A, Z, TKE, J, \pi)$, is required, that is the distributions in mass, charge, total kinetic energy, spin,

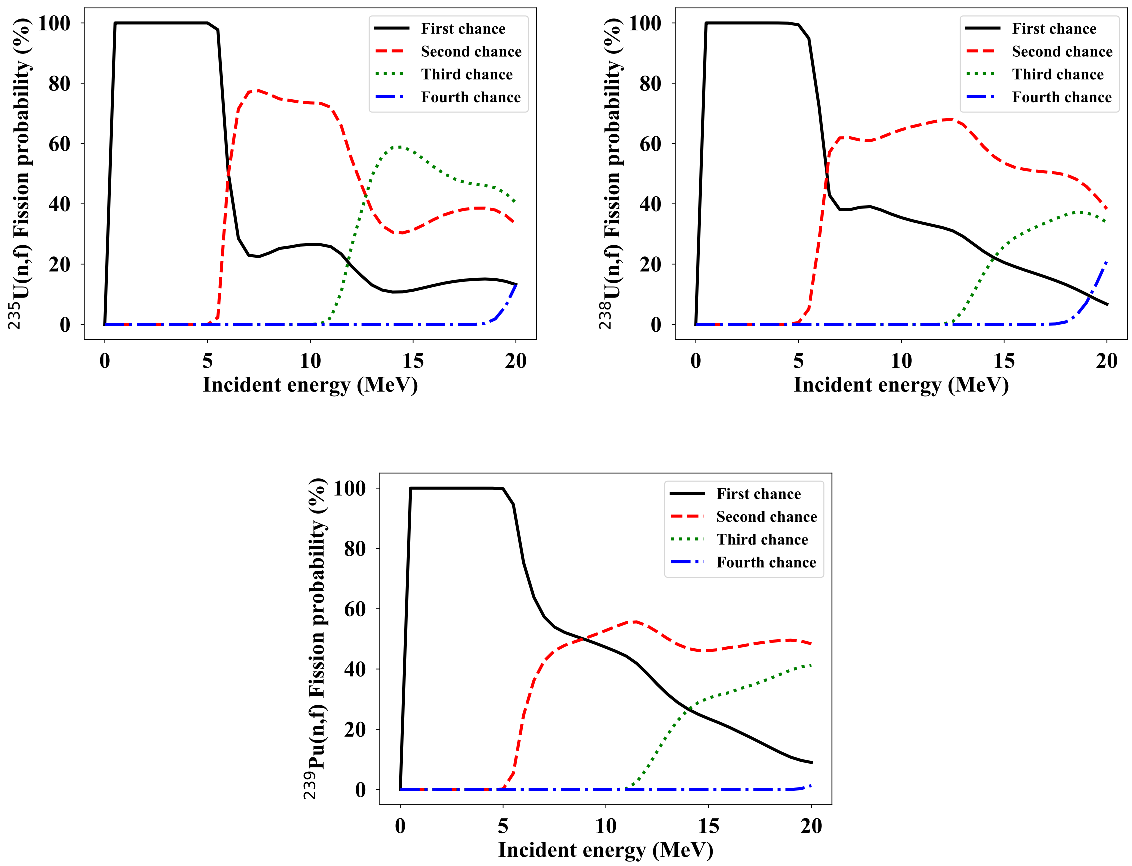

Figure 1: Multi-chance fission probabilities in `CGMF` calculated from `CoH3` for ^{235}U(n,f), ^{238}U(n,f), and ^{239}Pu(n,f).

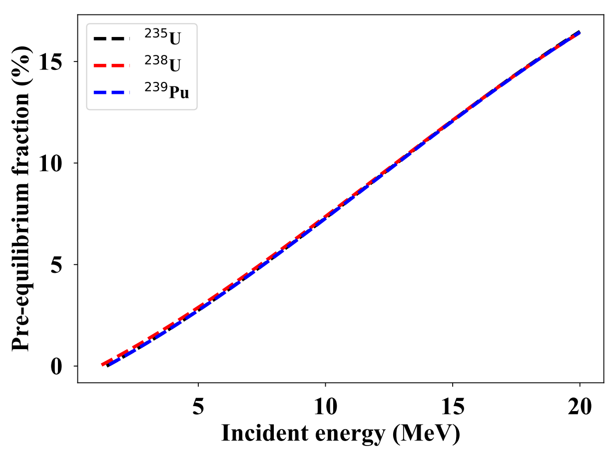

Figure 2: Fraction of first-emitted, pre-fission neutrons that are pre-equilibrium neutrons for ^{235}U(n,f), ^{238}U(n,f), and ^{239}Pu(n,f). Note that the three curves are essentially identical, as expected based on the similarities between the parameters in Table I.

Target	a_0	E_0	s $(\times 10^{-3})$	f_0
^{235}U	11.913	12.948	-9.6218	-0.294
^{238}U	11.913	12.948	-9.7463	-0.292
^{239}Pu	11.913	12.948	-9.6401	-0.294

Table I: Pre-equilibrium-fraction parameter values for Eq. (1).

and parity. The mass distribution is modeled as a sum of three Gaussian distributions,

$$Y(A|E_{\rm inc}) = G_0(A|E_{\rm inc}) + G_1(A|E_{\rm inc}) + G_2(A|E_{\rm inc}), \tag{2}$$

with

$$G_0(A|E_{\rm inc}) = \frac{W_0(E_{\rm inc})}{\sqrt{2\pi}\sigma_0(E_{\rm inc})} \exp\left[\frac{-(A-A_c/2)^2}{2\sigma_0(E_{\rm inc})^2}\right], \tag{3}$$

and

$$G_{1,2}(A|E_{\rm inc}) = \frac{W_{1,2}(E_{\rm inc})}{\sqrt{2\pi}\sigma_{1,2}(E_{\rm inc})} \left\{\exp\left[\frac{-(A-\mu_{1,2}(E_{\rm inc}))^2}{2\sigma_{1,2}(E_{\rm inc})^2}\right]\right. \tag{4}$$

$$\left. + \exp\left[\frac{-(A-(A_c-\mu_{1,2}(E_{\rm inc})))^2}{2\sigma_{1,2}(E_{\rm inc})^2}\right]\right\}. \tag{5}$$

Each of the weights, means, and widths are allowed to be energy-dependent with

$$W_{1,2}(E_{\rm inc}) = \frac{1}{1+\exp\left[(E_{\rm inc}-w^a_{1,2})/w^b_{1,2}\right]}, \tag{6}$$

$$\mu_i(E_{\rm inc}) = \mu_i^a + \mu_i^b E_{\rm inc}, \tag{7}$$

and

$$\sigma_i(E_{\rm inc}) = \sigma_i^a + \sigma_i^b E_{\rm inc}. \tag{8}$$

The weight of the symmetric mode is constrained by the normalization $2 = W_0 + 2W_1 + 2W_2$, and the width of the symmetric Gaussian mode is fixed at $\mu_0 = A_c/2$. The charge distribution, $Y(Z|A)$, is taken from Wahl systematics [6].

The average total kinetic energy, $\langle\mathrm{TKE}\rangle$, is linear in incident energy, with an inflection point reflective of the change in the slope of TKE($E_{\rm inc}$) seen experimentally for many isotopes. This is parametrized in `CGMF` as

$$\langle\mathrm{TKE}\rangle(E_{\rm inc}) = \begin{cases} a + bE_{\rm inc}, & \text{if } E_{\rm inc} \leq E_0 \\ c + dE_{\rm inc}, & \text{if } E_{\rm inc} \geq E_0 \end{cases} \tag{9}$$

where a, b, d, and E_0 are fitting parameters, and c is determined by the continuity at E_0,

$$c = a + (b-d)E_0. \tag{10}$$

Typically, E_0 is around 1 MeV. $\langle\mathrm{TKE}\rangle(E_{\rm inc})$ from `CGMF` compared to experimental data is shown in Fig. 3. The slope change in ^{235}U(n,f) and ^{238}U(n,f) around $E_{\rm inc} = 1$ MeV is visible in the experimental data—and absent for ^{239}Pu(n,f). In incident-energy ranges where the $\langle\mathrm{TKE}\rangle$ appears higher than the experimental data, the $\langle\mathrm{TKE}\rangle$ was adjusted to reproduce $\overline{\nu}(E_{\rm inc})$. However, large jumps in $\langle\mathrm{TKE}\rangle$ at the opening of the second-chance fission channel indicate that either the multi-chance fission probabilities or the TKE parametrizations need to be revisited.

The mass dependence of TKE is defined as polynomial,

$$\mathrm{TKE}(A) = \sum_{i=0}^{8} p_i (A - A_0)^i, \tag{11}$$

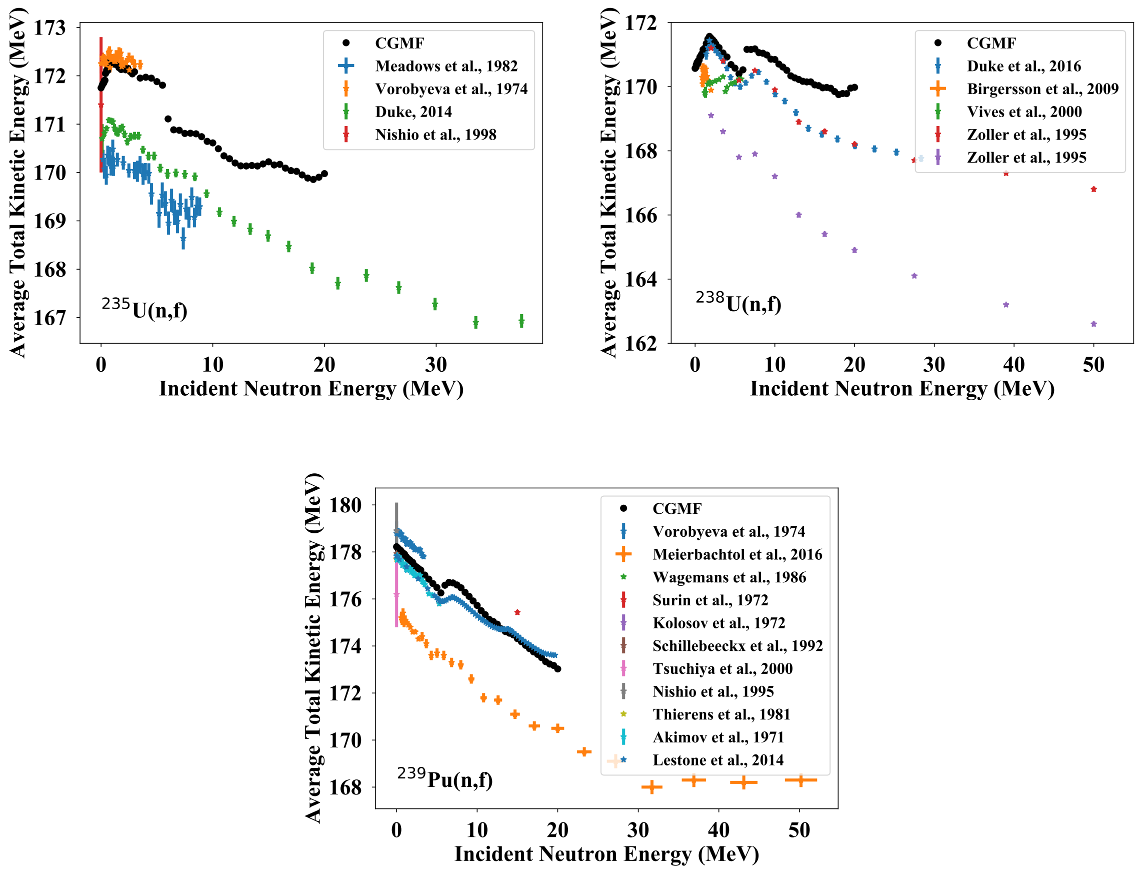

Figure 3: Average total kinetic energy from `CGMF` compared to experimental data for ^{235}U(n,f), ^{238}U(n,f), and ^{239}Pu(n,f).

and the width of the TKE distribution for each A-value is defined in a similar fashion,

$$\sigma_{\mathrm{TKE}}(A) = \sum_{i=0}^{8} s_i (A - A_0)^i. \tag{12}$$

In both cases, A_0 is a fitted expansion parameter—which can be different for both TKE(A) and $\sigma_{\mathrm{TKE}}(A)$, and typically one or more of the last s_i values are zero. In addition, because Eqs. (11) and (12) are polynomials, they can have unphysical values outside of the range over which they were fitted. For this reason, we also define A_{max} for TKE(A) and $\sigma_{\mathrm{TKE}}(A)$ as the maximum mass up to which this parametrization is valid, beyond which TKE(A) and $\sigma_{\mathrm{TKE}}(A)$ go to a pre-defined constant value. A_{max} can be different for both TKE(A) and $\sigma_{\mathrm{TKE}}(A)$. The total excitation energy, TXE, is determined based on the Q-value of the sampled split, TXE $= Q -$ TKE.

The spin distribution is defined proportionally to a Gaussian,

$$P(J) \propto (2J+1) \exp\left[\frac{-J(J+1)}{2B^2(Z,A,T)}\right], \tag{13}$$

where B^2 is the spin-cut off parameter, and the width of this distribution can be tuned with an energy-dependent parameter, $\alpha = \alpha_0 + \alpha_1 E_{\mathrm{inc}}$. Even and odd parity states are sampled with equal weight.

The parameters for the $Y(A)$, $Y(\mathrm{TKE})$, and $Y(J,\pi)$ models are given in Table II for ^{235}U, ^{238}U, and ^{239}Pu. This leaves 42 free parameters in the yield parametrization for each fissile target. When the

Parameter	^{235}U(n,f)	^{238}U(n,f)	^{239}Pu(n,f)
w_a^1	-6.856049	-2.167787	-25.369127
w_b^1	6.0824	5.0323	29.9818
μ_a^1	133.79	135.16	135.11
μ_b^1	-0.28	-0.09	0.13
σ_a^1	3.0288	3.3868	3.8465
σ_b^1	0.000	0.0142	0.0689
w_a^2	-6.863698	-2.224051	-25.258746
w_b^2	-6.1438	-5.1629	-30.0000
μ_a^2	140.97	142.20	141.35
μ_b^2	-0.27	-0.16	0.20
σ_a^2	4.6942	5.5624	6.5176
σ_b^2	0.1853	0.1048	0.0324
σ_a^0	9.8854	10.0092	9.9823
σ_b^0	0.0322	0.0153	0.0580
a	171.74	172.01	178.21
E_0	0.75	1.50	0.00
b	0.7181	0.0900	0.0000
d	-0.075	-0.3000	-0.3409
A_0(TKE)	131.70	130.00	131.49
$A_{\max}$(TKE)	166.00	162.00	170.00
p_0	1.7838×10^{2}	1.7774×10^{2}	1.8445×10^{2}
p_1	-3.8105×10^{-1}	2.4323×10^{-1}	-1.7386×10^{-1}
p_2	-1.4501×10^{-1}	-1.5521×10^{-1}	-9.4080×10^{-2}
p_3	5.9204×10^{-3}	4.0098×10^{-3}	3.7735×10^{-3}
p_4	2.0923×10^{-4}	1.7018×10^{-4}	-5.1130×10^{-5}
p_5	-1.6306×10^{-5}	-8.9348×10^{-6}	0.0
p_6	2.4070×10^{-7}	1.0190×10^{-7}	0.0
p_7	0.0	0.0	0.0
p_8	0.0	0.0	0.0
$A_0(\sigma_{\mathrm{TKE}})$	125.75	130.00	128.00
$A_{\max}(\sigma_{\mathrm{TKE}})$	163.00	162.00	159.00
s_0	9.3499	7.985	7.5837
s_1	-3.1996×10^{-1}	-2.0539×10^{-2}	1.0168×10^{-1}
s_2	4.1924×10^{-3}	-2.2611×10^{-2}	-1.6588×10^{-2}
s_3	1.9662×10^{-4}	1.2051×10^{-3}	3.9178×10^{-4}
s_4	-4.1142×10^{-6}	-1.6865×10^{-5}	0.0
s_5	0.0	0.0	0.0
s_6	0.0	0.0	0.0
s_7	0.0	0.0	0.0
s_8	0.0	0.0	0.0
α_0	1.45	1.5	1.53
α_1	0.070	0.071	0.071

Table II: Initial CGMF parameters for ^{235}U(n,f), ^{238}U(n,f), and ^{239}Pu(n,f).

energy of the incident neutron is above ~ 6 MeV, the second-chance fission channels opens, and above this energy range, both the compound, A, and $A-1$ systems can fission. The same parametrization can be used for the $A-1$ system (taking into account a shift in the compound mass), however, where there is experimental data, the parameters are tuned independently. Thus, as the multi-chance fission channels open (both second-chance fission and third-chance fission around 12 MeV), the number of free parameters is potentially doubled and then tripled. When experimental data are not available for the $A-1$ and $A-2$ systems, the parametrization of the A system is used, with A_c being shifted appropriately.

The TXE and TKE are then shared between the two fragments. The TXE is split between the fragments based on a ratio of temperatures,

$$R_T = \frac{T_L}{T_H} \approx \sqrt{\frac{U_L a_H(U_H)}{U_H a_L(U_L)}}, \tag{14}$$

where a_L (a_H) and U_L (U_H) are the level density and excitation energy of the light (heavy) fragment. In `CGMF` , R_T is implemented as a function of A to reproduce $\overline{\nu}(A)$, and U_L and U_H are iteratively searched over until Eq. (14) is fulfilled. The level densities are taken from the Fermi-gas model. Currently, R_T does not dependent on the incident-neutron energy, and $\overline{\nu}(A)$ only scales with the total prompt-neutron multiplicity. Then, TKE is split between the two fragments by conservation of energy.

To calculate the neutron evaporation from the fission fragments, neutron-transmission coefficients are required. The transmission coefficients for a certain channel, T_c, are calculated from the scattering matrix, S_{cc},

$$T_c = 1 - |\langle S_{cc}\rangle|^2 . \tag{15}$$

To calculate the transmission coefficients for all of the fission fragments that are produced during the fission processes, we rely on a global optical-model parametrization (OMP). The default OMP in `CGMF` is the Koning-Delaroche potential [7], a non-relativistic, spherical potential. Other global optical potentials are available—Refs. [8] and [9] are two examples of other common spherical potentials—and while these potentials lead to slight differences in the average energies of the neutrons emitted from the fission fragments, the PFNS calculated using all three are nearly identical, as seen in Fig. 4.

3 `CGMF` Model Parameter Selection

The neutron multiplicities and energies are not necessarily sensitive to all of the parameters described in Section 2. Therefore, we perform a sensitivity analysis for $\overline{\nu}$ and $\langle\varepsilon_n\rangle$ to each of these parameters in Table II for incident-neutron energies from thermal to 20 MeV. The sensitivities, R_{ij}, are defined as

$$R_{ij} = \frac{do_i}{dp_j}\frac{\overline{p}_j}{\overline{o}_i}, \tag{16}$$

where o is the observable (either $\langle\varepsilon_n\rangle$ or $\overline{\nu}$ at a single incident energy) and p is the parameter; $\overline{o}$ represents the observable calculated using the baseline values of the parameters, with $\overline{p}$ the default value of the parameter. Each parameter is initially varied by 2% to calculate the sensitivities. The initial parameters for each of the three isotopes studied in this report are listed in Table II. Note that a sensitivity was not calculated for any parameter listed as 0 in Table II.

The R_{ij} sensitivities are shown in Figs. 5, 6, and 7 for the parameters of ^{235}U(n,f), ^{238}U(n,f), and ^{239}Pu(n,f), respectively. It is important to note that these sensitivities only take into account the parametrization of the compound nucleus that is formed initially, and not the initial conditions of any of the compound nuclei that are formed at incident energies above ~ 6 MeV when the multi-chance fission channels begin to open. Looking at each of Figs. 5, 6, and 7, we see that $\langle\varepsilon_n\rangle$ and $\overline{\nu}$ are sensitive to the same parameters, and $\overline{\nu}$ is about five times as sensitive as $\langle\varepsilon_n\rangle$. Because of these trends in the

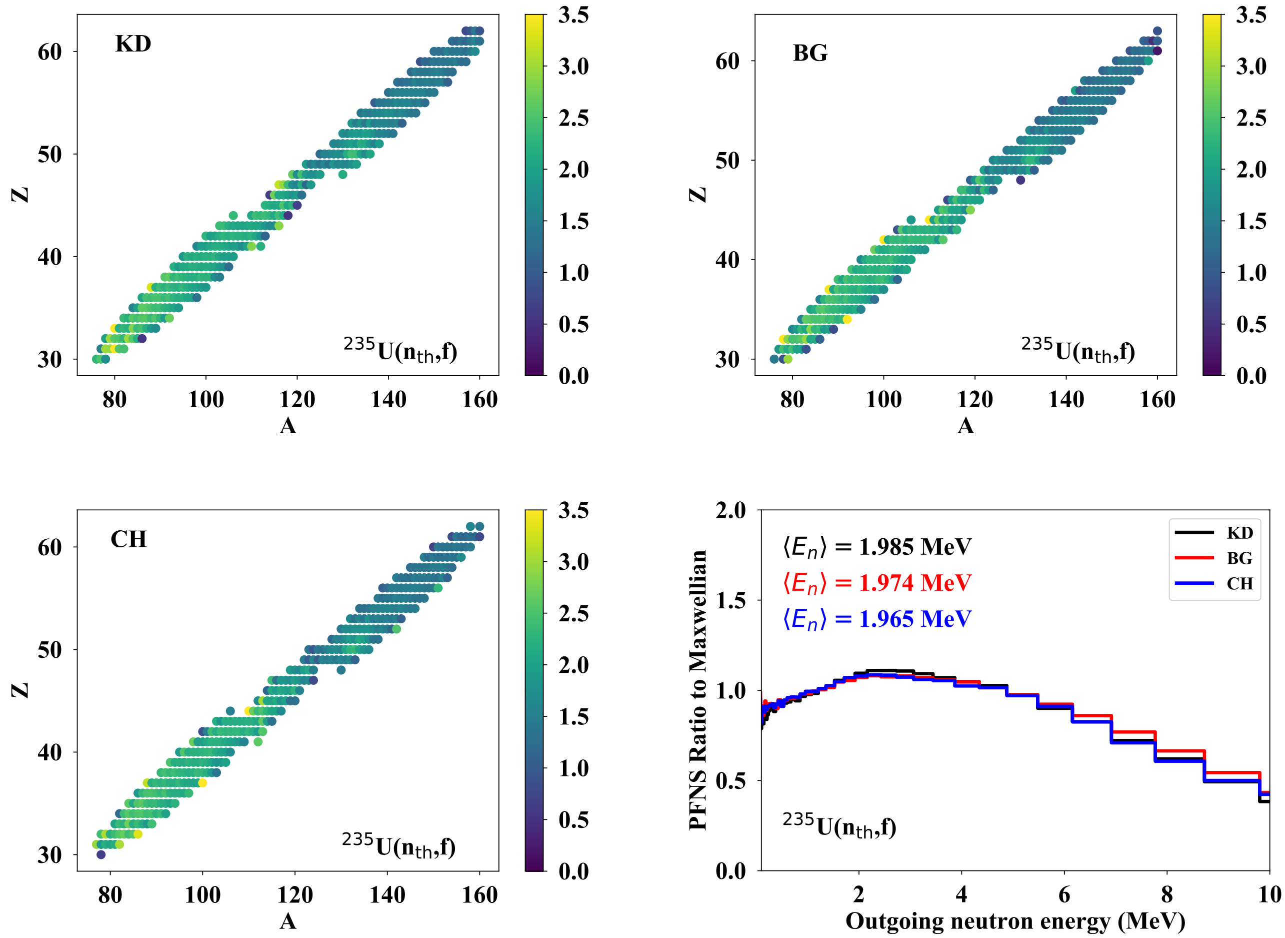

Figure 4: Average neutron energies emitted from the fission fragments for ^{235}U(n_{th},f) when the Koning-Delaroche (KD), Becchetti-Greenlees (BG), and Chapel-Hill 89 (CH) potentials are used to calculate the transmission coefficients for neutron evaporation, plus a comparison of the PFNS—as a ratio to a Maxwellian distribution (kT=1.32 MeV)—for the three optical potentials. Average neutron energies are listed in the colors corresponding to each given optical potential.

sensitivities, it becomes difficult to adjust both $\overline{\nu}$ and $\langle \varepsilon_n \rangle$ simultaneously. Small changes to $\overline{\nu}$ will have an even smaller effect on $\langle \varepsilon_n \rangle$, and as will be shown in Section 5, larger adjustments to the neutron energies are required. However, it is promising, from the consideration of calculation time, that these observables are strongly sensitive to only two to three parameters in the yield distribution.

It is important to note that in these studies, we have only focused on the parameters in the first-chance fission calculations, *e.g.*, for the ^{236}U compound but not the ^{235}U, ^{234}U, and ^{233}U compounds. Therefore, the parameter sensitivities shown in this section primarily concern incident energies lower than $\sim$ 6 MeV. Although there is some effect at higher incident energies (as shown in Figs. 5, 6, and 7), differences between $\overline{\nu}$ and the PFNS from `CGMF` values and experimental data will also depend on other parameters, such as fission barriers, which are not studied in detail in this report. Further studies will have to be performed to fully optimize all model parameters and consistently model the transitions between multi-chance fission channels.

We also have some indications that large changes in the spin-distribution cut-off parameter, α_0, can have a substantial effect on the mean neutron energy—and the shape of the PFNS. Therefore, a more sophisticated parameter optimization may be needed across the entire input space, where simultaneous, large changes in parameters can have compensating effects. However, a significant increase in α_0 comes at the cost of pushing the average γ-ray multiplicities to values higher than what are observed experimentally.

In addition, we then perform some bulk parameter studies for ^{235}U(n,f). Particularly seeing the spread of the experimental TKE values in Fig. 3, we increase and decrease the TKE by 1 MeV, through the a parameter in Eq. (9). The results of this tweaking is shown in Fig. 8 for $\langle$TKE$\rangle$, $\overline{\nu}$, and $\langle \varepsilon \rangle$, where the black curve shows the default `CGMF` calculation, red (blue) shows the results when TKE is increased (decreased) by 1 MeV. In addition, we change the multi-chance fission probabilities from those calculated by default in `CoH3` Miranda-3.5.3 to those calculated using the barriers from Ref. [4]. These different multi-chance fission probabilities are shown as the solid (default) and dashed (Ref. [4]) lines in the lower right panel of Fig. 8. The resulting $\langle$TKE$\rangle$, $\overline{\nu}$, and $\langle \varepsilon_n \rangle$ are shown in green in Fig. 8. Although the shift in the TKE by 1 MeV shows a much bigger change in $\overline{\nu}$ than $\langle \varepsilon_n \rangle$ (as expected from the sensitivity studies shown in Fig. 5), the changes in the multi-chance fission probabilities lead to a more significant change on the shape of the average neutron energies above the opening of second-chance fission.

We also see a large drop in the $\langle$TKE$\rangle$ as calculated by `CGMF` when the second-chance fission channel opens. This feature, which is not seen in the experimental data, is due to a combination of the change in the $\langle$TKE$\rangle$ parametrization between the ^{236}U and ^{235}U compound nuclei, the slope change in Eq. (9), and the very sharp increase in the second-chance fission probability. In addition, the kinks seen at the openings of multi-chance fission for $\overline{\nu}$ come from the differences in $\langle$TKE$\rangle$ for the ^{236}U, ^{235}U, and ^{234}U compounds, both the magnitude and slope of the parametrization. However, none of these bulk parameter tweaks change the shape of the tail of the PFNS in any significant manner.

4 Experimental-data Overview

`CGMF` model calculations and experimental data will be taken into account for the evaluations of PFNS and $\overline{\nu}$. To this end, all available experimental data will be extracted from EXFOR [10], their quality will be judged and covariances will be estimated for those data deemed reliable.

These steps were already undertaken for ^{235}U and ^{239}Pu PFNS as part of the evaluations documented in Ref. [4] and a recent in-house evaluation including Chi-Nu and CEA ^{239}Pu PFNS [11]. The experimental data shown in Tables III and IV encompass only these data that were judged to be of adequate quality for evaluation purposes. The uncertainties of these data displayed in figures in Section 5 are not the originally reported uncertainties but were changed by expert judgment to estimate suspected shortcomings in the data [12]. The only work that might need to be performed

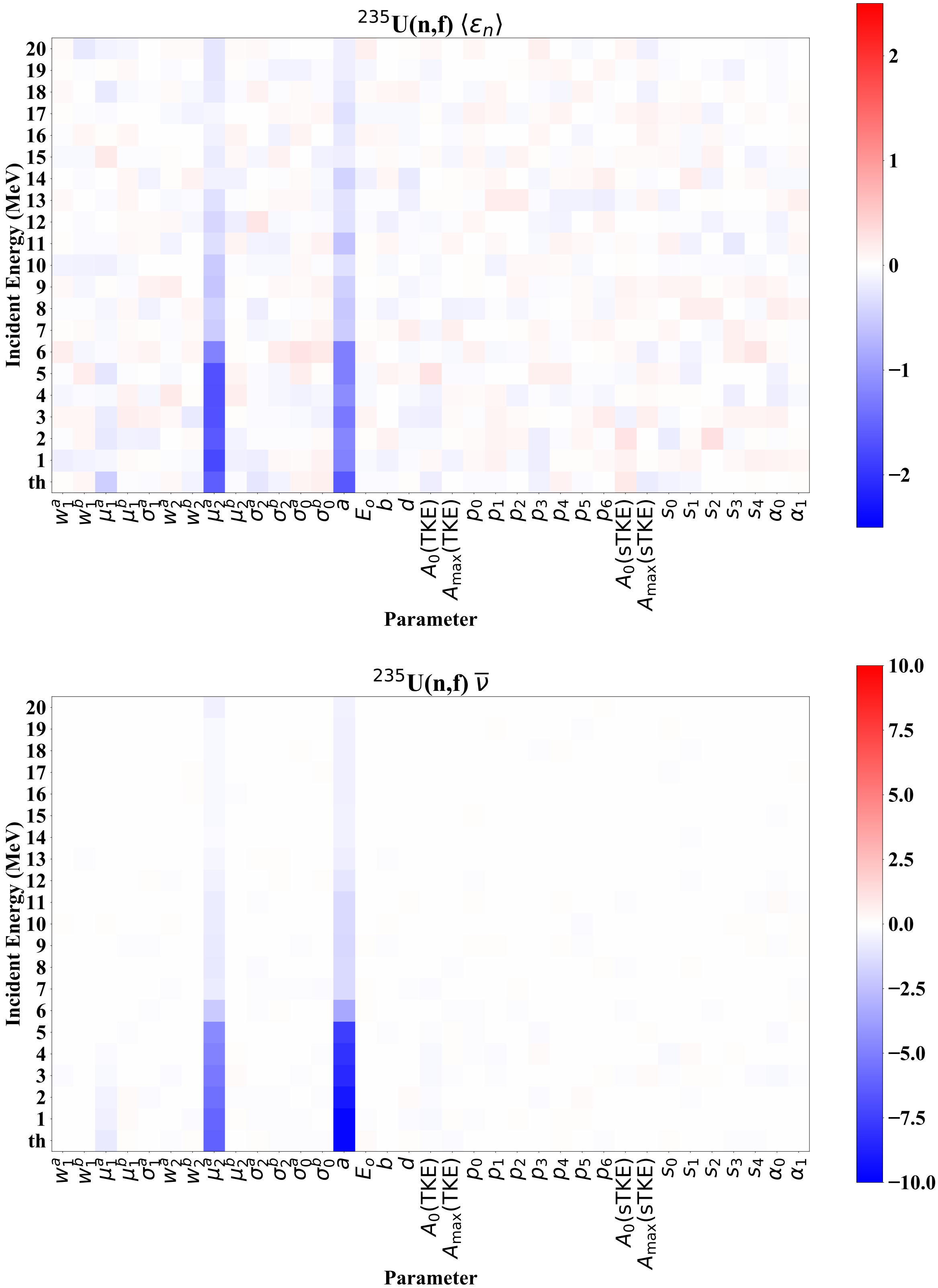

Figure 5: Sensitivities, R_{ij}, of (top) the mean energy of the PFNS and (bottom) average number of emitted neutrons for to the parameters in the yields, $Y(A, Z, \mathrm{TKE}, J, \pi)$, as a function of incident-neutron energy, for ^{235}U(n,f).

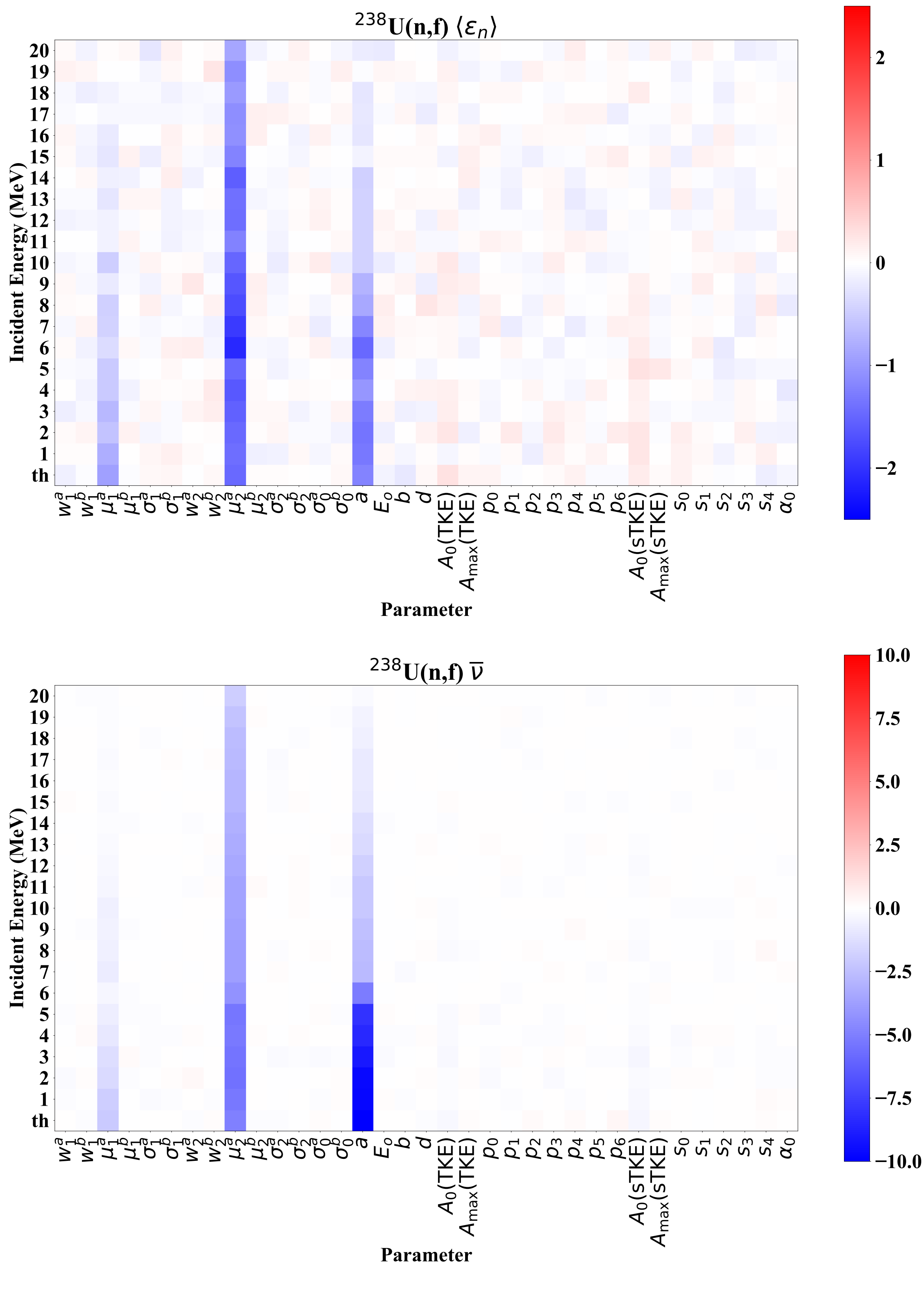

Figure 6: Sensitivities, R_{ij}, of (top) the mean energy of the PFNS and (bottom) average number of emitted neutrons for to the parameters in the yields, $Y(A, Z, \mathrm{TKE}, J, \pi)$, as a function of incident-neutron energy, for ^{238}U(n,f).

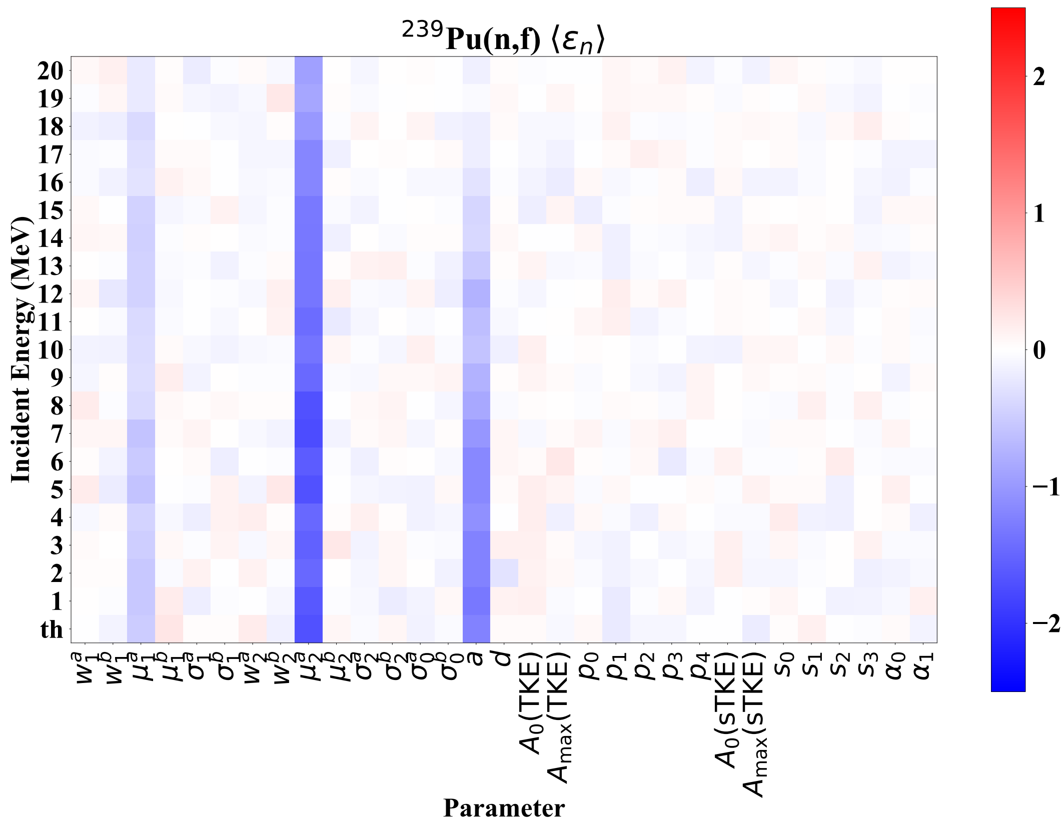

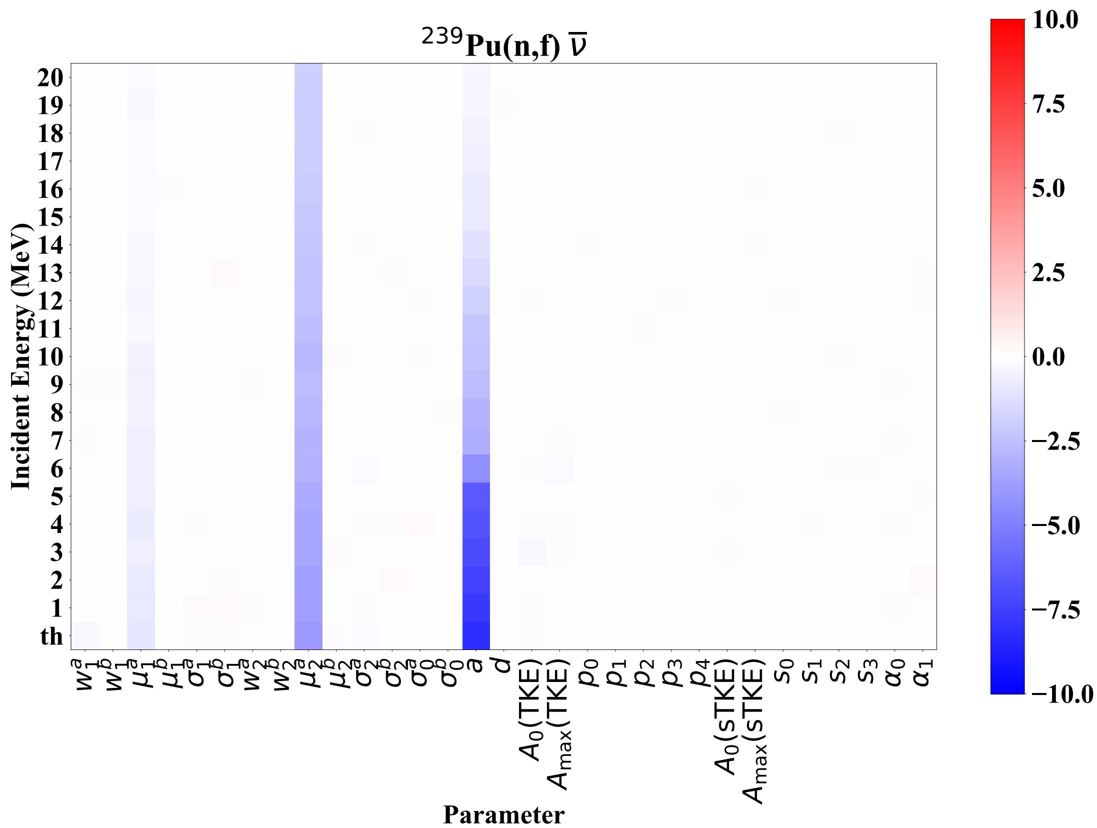

Figure 7: Sensitivities, R_{ij}, of (top) the mean energy of the PFNS and (bottom) average number of emitted neutrons for to the parameters in the yields, $Y(A, Z, \mathrm{TKE}, J, \pi)$, as a function of incident-neutron energy, for ^{239}Pu(n,f).

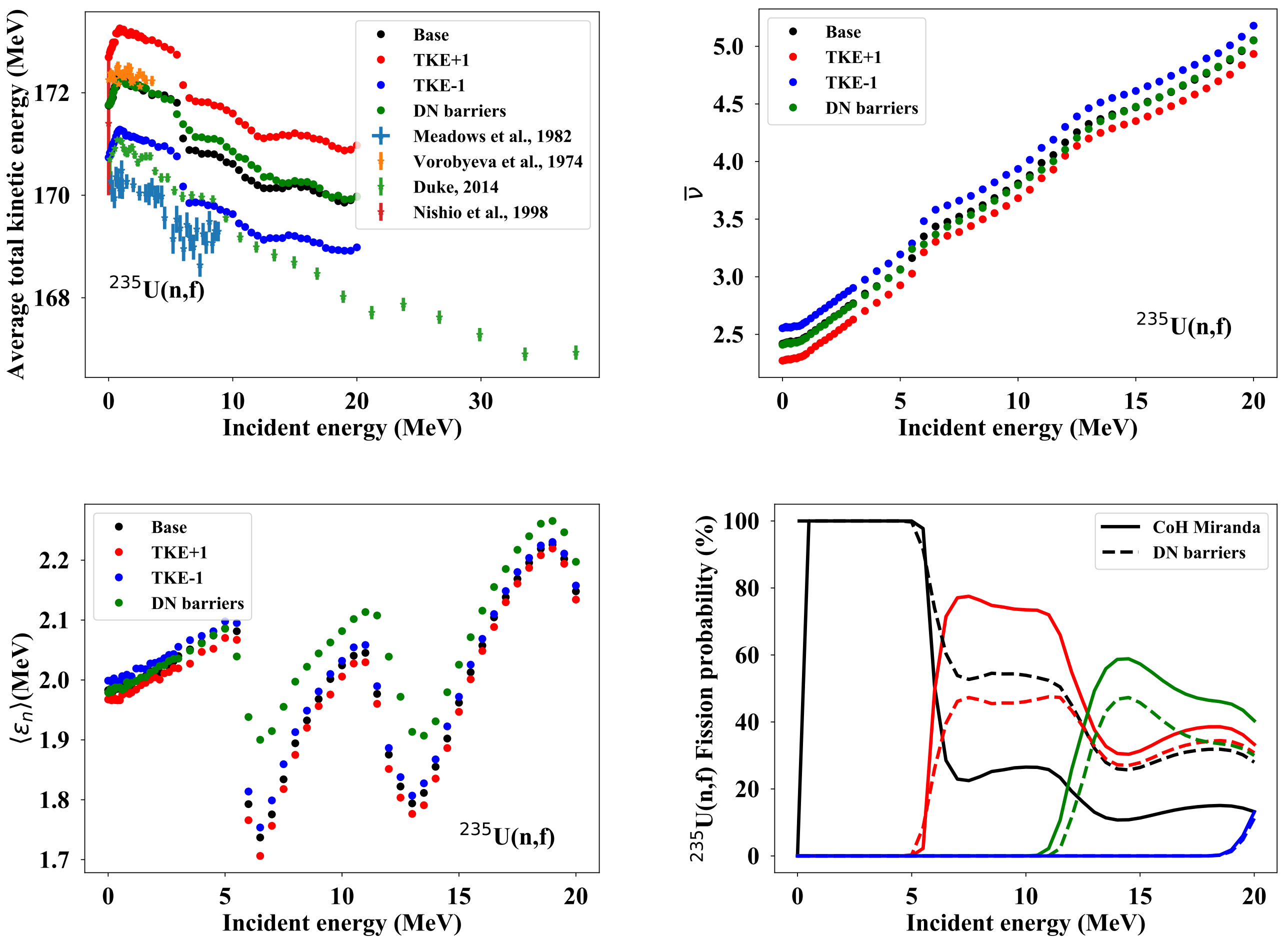

Figure 8: Changes in the CGMF results for ⟨TKE⟩, $\overline{\nu}$, and $\langle\varepsilon_n\rangle$ when TKE is increased by 1 MeV (red), TKE is decreased by 1 MeV (blue), and the multi-chance fission probabilities are changed (green), compared to the baseline CGMF calculation (black). The bottom right panel shows two different sets of multi-chance fission barriers, solid lines show the default CoH_3 calculations from the Miranda-3.5.3 version and the dashed lines show the multi-chance probabilities using the barriers from [4].

Table III: Measured differential PFNS data sets for neutron-induced fission of ^{235}U. The $E_{\rm inc}$ in MeV, EXFOR No., first author, year of publication and main reference, outgoing-neutron energy, E, and comments that include the quality of the information for the purposes of uncertainty quantification (UQ) are given. This table was taken from Ref. [13] and only those experiments are listed that will be used for the actual evaluation.

$E_{\rm inc}$	EXFOR	First Author & Year	Type of data	E (MeV)	Comments
thermal	41597002	Vorobyev (2013) [14]	ratio to Cf	0.221–16.65	Detailed UQ
thermal	31692006	Kornilov (2011) [15]	ratio to Cf	0.7–11.8	Detailed UQ
thermal	40871011	Nefedov (1983) [16]	ratio to Cf	0.084–0.91	Detailed UQ
thermal	40871012	Nefedov (1983) [16]	ratio to Cf	1.0–7.8	Detailed UQ
thermal	40872007	Starostov (1983) [17]	ratio to Cf	4.115–12.06	Detailed UQ
thermal	40873004	Boytsov (1983) [18,19]	ratio to Cf	0.021–4.5	Detailed UQ
1.5	–	Lestone (2014) [20,21]	shape	1.5–11.5	Detailed UQ
2.9	41110009	Boykov (1991,1994) [22,23]	ratio to Cf	0.232–11.885	Detailed UQ
0.53	20175003	Johansson (1977) [24,25]	shape	0.625–14.45	Incomplete UQ
0.4	20385003	Islam (1973) [24,27]	shape	0.58–6.9	Incomplete UQ
1.5	20394008	Knitter (1972) [26]	shape	1.8–6.7	Incomplete UQ
1.5–20	–	Chi-Nu (2018) [5]	ratio to fct.	0.01–2.1	to be finalized

for experimental PFNS of these two isotopes is including the newest data of the Chi-Nu collaboration when delivered.

Table IV: Experimental PFNS for neutron-induced fission of ^{239}Pu. The incident-neutron energy, E_{inc} (MeV), EXFOR No., first author, year of publication and main reference, type of data, outgoing-neutron energy, E, and comments that include the quality of the information for the purposes of UQ are given. This table was taken from Ref. [13] and only those experiments are listed that will be used for the actual evaluation.

E_{inc}	EXFOR	First Author & Year	Type of data	E (MeV)	Comments
thermal	40871009	Nefedov (1983) [16]	ratio to Cf	0.08–1.8	Detailed UQ
thermal	40871010			1.2–9.1	
thermal	40872006	Starostov (1983) [17]	ratio to Cf	3–11.2	Detailed UQ
thermal	40873006	Boytsov (1983) [18]	ratio to Cf	0.02–4.5	Incomplete UQ
thermal	40930	Starostov (1985) [19]	ratio to Cf	0.02-11.2	Incomplete
thermal	30704004	Lajtai (1985) [28]	ratio to Cf	0.03–3.9	Detailed UQ (Cf) [29]
1.5	–	Lestone (2014) [20,21]	shape	1.5–11.5	Detailed UQ
1–200	14379	Chatillon (2014) [30,31]	shape	0.3–8.3	Detailed UQ
0.215	20576003	Knitter (1975) [24,32]	shape	0.28–13.9	Incomplete UQ
1–28	–	CEA (2020) [33]	ratio to Cf	0.25–11.3	Incomplete UQ
1.5–19	–	Chi-Nu (2020)	ratio to fct.	0.01–9.4	Detailed UQ

As part of this project, ^{238}U PFNS listed in Table V will need to be extracted from EXFOR. Their uncertainties will be estimated using the code ARIADNE [34]. Correlations will be estimated between uncertainties of the same and different experiments. To this end, the literature and EXFOR entries will be studied in detail to glean an understanding of potential biases in the data, but also to extract pertinent uncertainty sources (*e.g.*, counting statistics, background, multiple scattering and attenuation, detector response, angular distribution of fission fragments and neutrons, nuclear data, time resolution and TOF length uncertainties). Uncertainties that were not provided in EXFOR or literature but are clearly missing will be estimated by taking recourse to templates of expected uncertainties in PFNS measurements [35]. Experimental uncertainties and associated correlation coefficients will then be estimated for each pertinent uncertainty source based on this information following the procedure outlined in Ref. [4, 13].

Table V: Experimental PFNS for fast neutron-induced fission of ^{238}U. The incident-neutron energy, E_{inc}, in MeV, EXFOR [10] accession number, first author, year of publication and main reference, type of data, outgoing-neutron energy, E, and comments that include the quality of the information for the purposes of UQ are given. This table was taken from Ref. [13].

E_{inc}	EXFOR	First Author, Year	Type of data	E (MeV)	Comments
14.3	40740002	Baryba (1979) [36, 37]	shape	0.6–9.96	Incomplete UQ
6.01	40631	Kornilov (1980) [37, 38]	shape	0.72–8.8	Incomplete UQ
7.02				0.62–8.14	
8.01				0.7–8.63	
8.94				0.61–9.73	
2.0	22112003	Baba (1989) [39]	shape	2.3–12.87	Incomplete UQ
2.9	41110010	Boykov* (1991) [22, 23, 40]	shape, ratio to Cf	0.232–11.885	Incomplete UQ
14.7			shape, ratio to Cf	0.225–11.77	
16.0	41461004	Smirenkin (1996) [41]	shape, ratio to Cf	0.39–11.95	Incomplete UQ
17.7				0.39–13.36	
5.0	41450003	Trufanov (2001) [42]	shape, ratio to Cf	0.28–12.27	Incomplete UQ
13.2			shape, ratio to Cf	0.45–12.36	
6.0	41447003	Lovchikova (2004) [43]	shape, ratio to Cf	0.13–13.77	Incomplete UQ
7.0			shape, ratio to Cf	0.14–15.17	
2.0	33084	Desai (2015) [13, 44]	shape	0.75–8.75	Incomplete UQ
2.5			shape	0.75–6.75	
3.0			shape	0.75–8.25	

The data for ^{235,238}U(n,f) and ^{239}Pu(n,f) $\overline{\nu}$ listed in Tables VI–VIII have been extracted from EXFOR. An uncertainty estimate will be started for ^{239}Pu(n,f) $\overline{\nu}$ data in FY20 and will need to be finished in FY21. Covariances will need to be estimated for ^{235}U(n,f) and ^{238}U(n,f) $\overline{\nu}$ as well. To this end, a module will be developed in the code package ARIADNE to estimate experimental covariances for $\overline{\nu}$ measurements. Similarly to PFNS measurements, uncertainty values, δ_i^k, and correlation coefficients, $\mathrm{Cor}_{i,j}^k$, will be estimated for each expected uncertainty source k at incident-neutron energy i or j. Total covariances, $\mathrm{Cov}_{i,j}^{tot}$, will then be estimated by:

$$\mathrm{Cov}_{i,j}^{tot} = \sum_k \delta_i^k \mathrm{Cor}_{i,j}^k \delta_j^k, \tag{17}$$

assuming that the individual uncertainty sources are partitioned such that they be independent. A template of expected uncertainties was recently developed for absolute and ratio $\overline{\nu}$ measurements [35] and will be used to estimate comprehensive covariances for all data sets accepted for evaluation purposes. Correlation coefficients will be provided for uncertainties for the same and between different experiments.

Table VI: Measured $\overline{\nu}$ data sets for ^{235}U(n,f) found in EXFOR. The EXFOR No., first author, year of publication and E_{inc} are given.

EXFOR no.	First Author & Year	Monitor	E_{inc} (MeV)
41673.003	Apalin 1962	N/A	$2.53e^{-8}$
41397.01	Apalin 1965	N/A	$2.53e^{-8}$
21139.003	Barnard 1965	N/A	$2.53e^{-8}$
12397.002	Bethe 1955	N/A	4–4.5
40158.006	Bljumkina 1964	^{235}U(n,f) $\overline{\nu}_t$	0.08–0.99
41110.006	Boikov 1991	^{252}Cf(sf) $\overline{\nu}_p$	2.9–14.7

30772.003	Boldeman 1985	^{252}Cf(sf) $\overline{\nu}_p$	$2.53e^{-8}$
21454.005/7/8	Colvin 1965	^{252}Cf(sf) $\overline{\nu}_p$	$2.53e^{-8}$–2.57
20025.002	Conde 1965	^{252}Cf(sf) $\overline{\nu}_p$	7.5–14.8
14294.002	DeVolpi 1966	N/A	$2.53e^{-8}$
12337.003	Diven 1956	^{235}U(n,f) $\overline{\nu}_p$	0.08
12436.002	Diven 1957	N/A	1.25–4.8
14297.007	Diven 1961	^{252}Cf(sf) $\overline{\nu}_p$	4
14297.006	Diven 1961(2)	^{252}Cf(sf) $\overline{\nu}_t$	$2.53e^{-8}$
21252.005	Fieldhouse 1966	^{252}Cf(sf) $\overline{\nu}_t$	0.075–14.2
21252.006	Fieldhouse 1966(2)	^{252}Cf(sf) $\overline{\nu}_t$	0.04–7.96
40806.003	Flerov 1958	N/A	14.1
22592.003	Frehaut 1973	^{252}Cf(sf) $\overline{\nu}_t$	$2.00e^{-6}$–$4.46e^{-5}$
20506.002	Frehaut 1980	^{252}Cf(sf) $\overline{\nu}_t$	1.36–14.79
21685.002	Frehaut 1980(2)	^{252}Cf(sf) $\overline{\nu}_t$	2.279–2.828
21785.003	Frehaut 1982	^{252}Cf(sf) $\overline{\nu}_t$	1.14–14.66
12345.003	Fultz 1966	N/A	$2.53e^{-8}$
12833.001/3+12906.003	Gwin 1984	^{252}Cf(sf) $\overline{\nu}_t$	$2e^{-8}$–$4.1e^{-5}$
13101.003	Gwin 1986	^{252}Cf(sf) $\overline{\nu}_p$	0.0005–9
12326.004	Hopkins 1963	^{252}Cf(sf) $\overline{\nu}_t$	$2.53e^{-8}$–14.5
10574.003	Howe 1976	^{235}U(n,f) $\overline{\nu}_t$	$5.20e^{-7}$–$8.43e^{-5}$
14051.002	Howe 1976(2)	^{252}Cf(sf) $\overline{\nu}_t$	$8.90e^{-2}$–23.3
12870.004	Howe 1984	^{235}U(n,f) $\overline{\nu}_p$	17–48.9
21696.004	Johnstone 1956	^{235}U(n,f) $\overline{\nu}_t^M$	2.5–14.1
20427.002	Kaeppeler 1975	^{235}U(n,f) $\overline{\nu}_p$	0.225–1.363
40356.003	Kalashnikova 1957	^{235}U(n,f) $\overline{\nu}_t^M$	$2.53e^{-8}$
33102.004	Kappor 1963	N/A	$2.53e^{-8}$
41378.002	Khoklov 1994	^{252}Cf(sf) $\overline{\nu}_p$	0.048–14.122
12419.002	Meadows 1962	^{252}Cf(sf) $\overline{\nu}_p$	0.03–1.76
12391.002	Meadows 1965	^{252}Cf(sf) $\overline{\nu}_t$	3.91–6.36
12399.002/4	Meadows 1967	^{252}Cf(sf) $\overline{\nu}_t$	0.039–1
30022.002	Nadkarni 1967	N/A	0.37–2.13
40871.003	Nefedov 1983	^{252}Cf(sf) $\overline{\nu}_p$	$2.53e^{-8}$
40033.002/4/6/8	Nesterov 1970	^{252}Cf(sf) $\overline{\nu}_p$	$2.53e^{-8}$–1.51
40132.002	Prokhorova 1967	^{235}U(n,f) $\overline{\nu}_p$	0.37–3.25
40392.002/3	Protopopov 1958	^{235}U(n,f) $\overline{\nu}_p^M$	14.8
10427.003	Reed 1973	^{235}U(n,f) $\overline{\nu}_p^M$	$1.20e^{-8}$–$2.64e^{-5}$
21456.005	Sanders 1956	N/A	$2.53e^{-8}$
40058.004	Savin 1970	^{252}Cf(sf) $\overline{\nu}_p$	0.65–6.6
40262.002	Savin 1972	^{252}Cf(sf) $\overline{\nu}_p$	0.86–5.35
40493.002	Savin 1979	^{252}Cf(sf) $\overline{\nu}_p$	0.198–0.985
20600.002	Simon 1976	^{252}Cf(sf) $\overline{\nu}_p$	$2.03e^{-6}$–$7.46e^{-5}$
40388.006	Smirenkin 1958	^{235}U(n,f) $\overline{\nu}_p^M$	4–15
12395.002	Snyder 1944	N/A	$2.53e^{-8}$
20568.002	Soleihac 1970	^{252}Cf(sf) $\overline{\nu}_p$	0.223–1.87
40785.002	Vasilev 1960	N/A	14.3
41597.004	Vorobyev 2013	N/A	$3.63e^{-8}$
30006.002	Walsh 1971	^{252}Cf(sf) $\overline{\nu}_p$	0.11–1.9
20113.003	Widen 1973	^{252}Cf(sf) $\overline{\nu}_p$	$2.53e^{-8}$

Table VII: Measured $\overline{\nu}$ data sets for ^{238}U(n,f) found in EXFOR. The EXFOR No., first author, year of publication and E_{inc} are given.

EXFOR no.	First Author & Year	Monitor	E_{inc} (MeV)
20075.002	Asplund 1964	^{252}Cf(sf) $\overline{\nu}_p$	1.49–14.8
21139.002	Barnard 1965	N/A	2.09–4.91
40740.003	Baryba 1979	^{252}Cf(sf) $\overline{\nu}_p$	14.3–14.3
12397.004	Bethe 1955	N/A	4.5
41110.007	Boikov 1991	^{252}Cf(sf) $\overline{\nu}_p$	2.9–14.7
40671.003	Bondarenko 1958	^{235}U(n,f) $\overline{\nu}_p$	4
12462.002	Butler 1961	^{235}U(n,f) $\overline{\nu}_p$	1.58
20072.003	Conde 1961	^{252}Cf(sf) $\overline{\nu}_p$	3.6–14.9
33084.003	Desai 2015	^{252}Cf(sf) $\overline{\nu}_p$	2–3
21696.005	Diven 1956	^{235}U(n,f) $\overline{\nu}_t^M$	2–14.1
12436.003	Diven 1958	N/A	1.5
21252.004	Fieldhouse 1966	^{252}Cf(sf) $\overline{\nu}_p$	14.2
40806.005	Flerov 1958	N/A	14.1
20490.002	Frehaut 1980	^{252}Cf(sf) $\overline{\nu}_p$	1.36–14.79
21685.003	Frehaut 1980 (2)	^{252}Cf(sf) $\overline{\nu}_p$	22.79–28.28
21696.005	Johnstone 1956	^{235}U(n,f) $\overline{\nu}_t^M$	2.5–14.1
40631.006	Kornilov 1980	^{252}Cf(sf) $\overline{\nu}_t$ DE	6.01–8.94
41213.003	Kuzminov 1961	^{235}U(n,f) $\overline{\nu}_p$	2.3–3.75
14384.002	Laurent 2014	N/A	1.4–19.11
21453.002	Leroy 1960	^{235}U(n,f) $\overline{\nu}_p$	14.2
21135.006	Mather 1965	^{252}Cf(sf) $\overline{\nu}_t$	1.4–4.02
40429.003	Nurpeisov 1975	^{252}Cf(sf) $\overline{\nu}_t$ DE	1.2–4.89
40138.002	Sabin 1972	^{252}Cf(sf) $\overline{\nu}_p$	1.27–5.87
14296.002	Sher 1960	N/A	2.8
41461.003	Smirenkin 1996	^{252}Cf(sf) $\overline{\nu}_p$ DE	16–17.7
14215.003	Taieb 2007	N/A	1.76–190.01
40785.003	Vasilev 1960	N/A	14.3
21094.007	Voignier 1968	N/A	14.1
40665.002	Vorobyeva 1981	^{252}Cf(sf) $\overline{\nu}_p$	1.3–5.89
21909.003	Yamamoto 1979	N/A	14.5
32606.002	Zangyou 1975	^{240}Pu(sf) $\overline{\nu}_t$	1.22–5.5

Table VIII: Measured $\overline{\nu}$ data sets for ^{239}Pu(n,f) found in EXFOR. The EXFOR No., first author, year of publication, main reference and E_{inc} are given.

EXFOR no.	First Author & Year	Monitor	E_{inc} (MeV)
41397.008	Apalin 1965	N/A	2.53e^{-8}
30772.004	Boldeman 1980 [45]	^{252}Cf(sf) $\overline{\nu}_p$	2.53e^{-8}
20052.002	Conde 1968 [46]	^{252}Cf(sf) $\overline{\nu}_p$	4.22–14.8
12337.004	Diven 1956 [47]	^{235}U(n,f) $\overline{\nu}_p$	0.08
14279.009 +.010	Diven 1961 [47]	^{252}Cf(sf) $\overline{\nu}_t$	2.53e^{-8}–4
20490.003	Frehaut 1973 [48]	^{252}Cf(sf) $\overline{\nu}_p$	1.36–14.79
21685.004	Frehaut 1980 [48]	^{252}Cf(sf) $\overline{\nu}_p$	22.79–28.28
10759.004	Gwin 1978 [49]	^{252}Cf(sf) $\overline{\nu}_p$	5e^{-5}–6.4

12906.002	Gwin 1984 1 [49]	^{252}Cf(sf) $\overline{\nu}_p$	5e^{-9}–6e^{-5}
12833.004	Gwin 1984 2 [49]	^{252}Cf(sf) $\overline{\nu}_p$	5e^{-9}–1e^{-5}
13101.004	Gwin 1986 [49]	^{252}Cf(sf) $\overline{\nu}_p$	5e^{-4}–10
12326.005+.006	Hopkins 1963 [50]	^{252}Cf(sf) $\overline{\nu}_p$	2.53e^{-8}–14.5
30600.002	Huanqiao 1980 [51]	^{1}H(n,el) cs	0.186–1.44
21696.006	Johnstone 1965 [52]	^{235}U(n,f) $\overline{\nu}_t^M$	14.1
40757.002	Kalashnikova 1955 [53]	N/A	2.53e^{-8}
40523.002	Khoklov 1976 [54]	^{252}Cf(sf) $\overline{\nu}_t$	1.06–1.81
21453.004	Leroy 1960 [55]	^{238}U(n,f) $\overline{\nu}_p$	14.2
21135.007+008	Mather 1965 [56]	^{252}Cf(sf) $\overline{\nu}_t$	2.53e^{-8}–4.02
40871.002	Nefedov 1983	^{252}Cf(sf) $\overline{\nu}_p$	2.53e^{-8}
4033.003+.007	Nesterov 1970 [57]	^{252}Cf(sf) $\overline{\nu}_p$	2.53e^{-8}–1.607
23012.009	Nishio 1988	N/A	2.53e^{-8}
40429.004	Nurpeisov [58] 1975	^{252}Cf(sf) $\overline{\nu}_p$	0–4.89
21456.007	Sanders 1956	^{235}U(n,f) $\overline{\nu}_p^M$	2.53e^{-8}
40058.003	Savin 1970 [59]	^{252}Cf(sf) $\overline{\nu}_p$	0.89–4.7
40388.007	Smirenkin 1959 [60]	^{239}Pn(n,f) $\overline{\nu}_p^M$	4–15
20568.004	Soleihac 1970 [61]	^{252}Cf(sf) $\overline{\nu}_p$	0.21–1.375
40148.003	Volodin 1970 (1) [62]	^{252}Cf(sf) $\overline{\nu}_p$	2.53e^{-8}–1.6
40148.005	Volodin 1970 (2) [62]	^{239}Pu(n,f) $\overline{\nu}_p^M$	0.08–0.7
41611.008	Vorobyev 2016	N/A	thermal spectrum
30006.004	Walsh1970 [63]	^{252}Cf(sf) $\overline{\nu}_p$	0.2–1.9

5 Challenges to Overcome and Agreement of Model Calculations with Experimental Data

Each `CGMF` run takes between 1 and 5 minutes using 100 cores (3 nodes) on the LANL computational cluster Snow, for 100,000 to 500,000 fission events. 500,000 fission events were shown to be necessary for a converged PFNS calculation. On Snow, the maximum nodes per user is 20, so this computing time could be decreased as well to run further sensitivities or parameter sampling. In addition, we have the option of using the deterministic fission-decay code `BeoH` [64], which calculates the PFNS and $\overline{\nu}$ as well. Without considering the MPI implementation of `CGMF`, `BeoH` takes less time to run for a converged PFNS result (*e.g.*, about 20 minutes for yields on the order of 10^{-5} to be computed at thermal incident-neutron energy). However, when taking into account the parallelization of `CGMF`, and that `BeoH` has not been parallelized, `CGMF` is faster. In addition, while the models within `CGMF` and `BeoH` are similar, the conversion of the calculated center-of-mass PFNS to the lab frame PFNS within `BeoH` is only approximate at incident-neutron energies beyond second-chance fission; in `CGMF`, this transformation is exact, because the neutron energies are converted from center-of-mass to lab frame on an event-by-event basis. Therefore, we do not suggest using `BeoH` for this study.

It is obvious from both, the mean energies of the PFNS and the PFNS itself (shown in Figs. 9–16 for ^{235,238}U and ^{239}Pu), that the current version of `CGMF` using the initial parameter sets is not able to predict a PFNS in agreement with existing experimental or evaluated data (ENDF/B-VIII.0, JEFF-3.2 or JENDL-4.0).

The `CGMF` PFNS calculated with the initial parameter sets is systematically too low compared to experimental data for all isotopes studied and at all incident-neutron energies. Originally, unexpected structures were observed for ^{239}Pu PFNS at all incident-neutron energies below 300 keV in Figs. 15–16 that increased in magnitude with E_{inc}. Similar structure are observed for the ^{235}U PFNS in Fig. 12. These structures did not vanish with increasing number of events (up to 2 million events). The major structures were due to the binning of the excitation energies in the compound nuclei when pre-fission

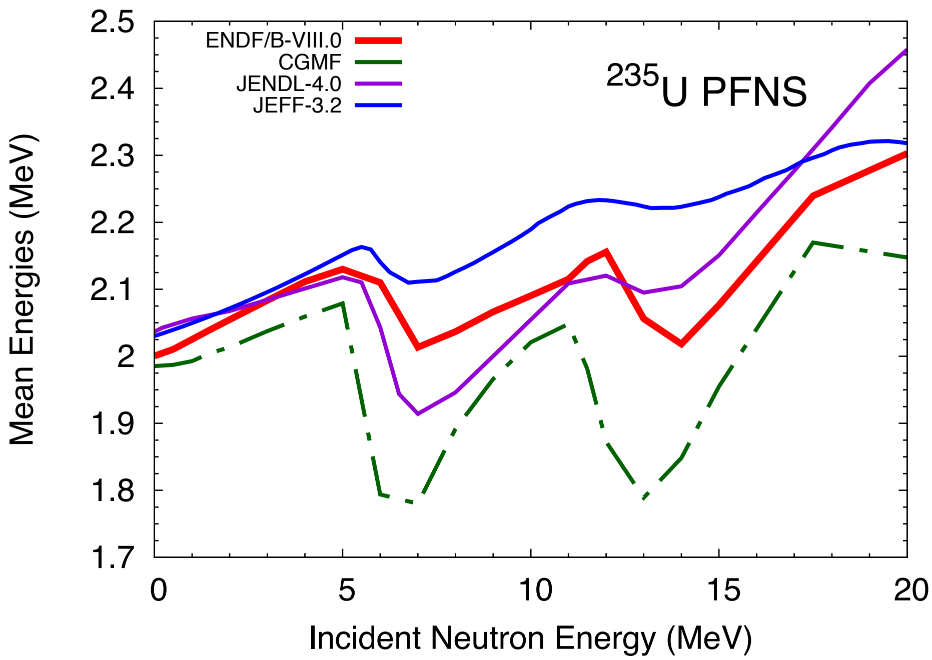

Figure 9: The mean energies of the ^{235}U PFNS calculated with CGMF are compared to those reported for ENDF/B-VIII.0, JENDL-4.0 and JEFF-3.2.

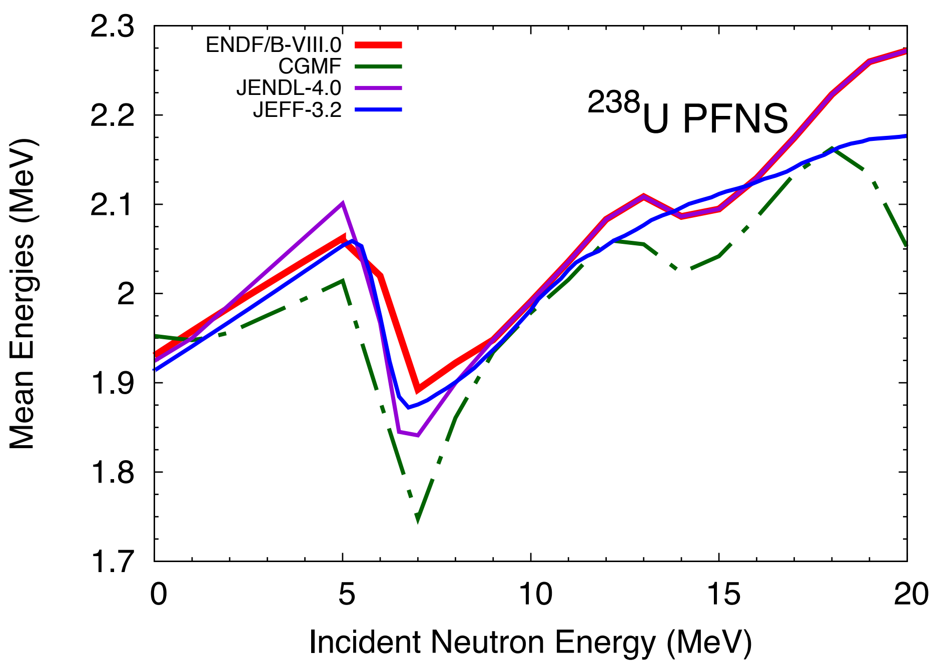

Figure 10: The mean energies of the ^{238}U PFNS calculated with CGMF are compared to those reported for ENDF/B-VIII.0, JENDL-4.0 and JEFF-3.2.

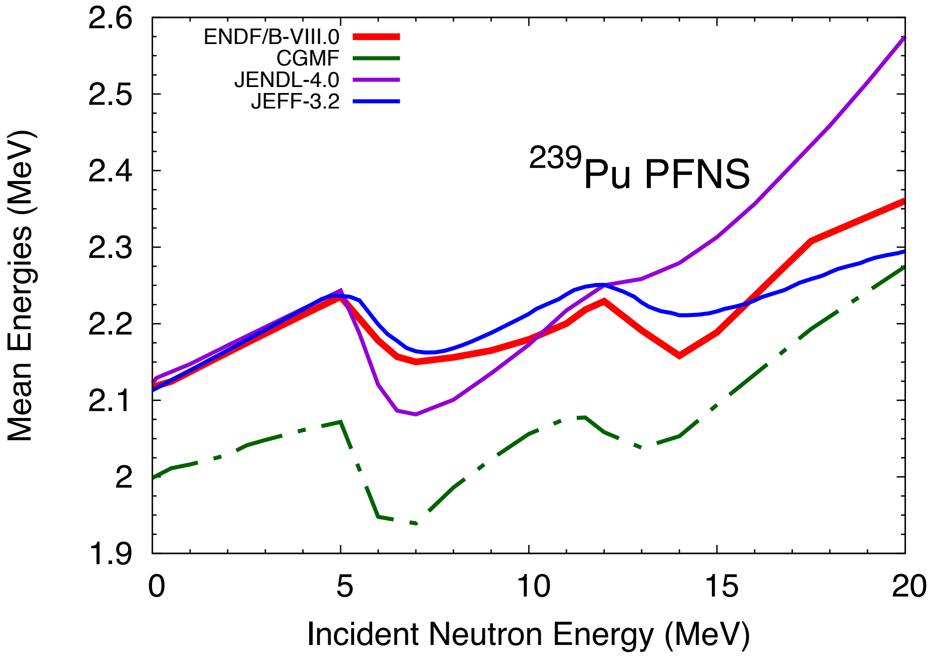

Figure 11: The mean energies of the ^{239}Pu PFNS calculated with CGMF are compared to those reported for ENDF/B-VIII.0, JENDL-4.0 and JEFF-3.2.

neutrons were emitted. These were resolved by T. Kawano and I. Stetcu by adding a random number within the size of the bin to the sampled pre-fission neutron energy. Distinctly smaller structures remain that could be attributed to the outgoing-neutron energy binning that still need to be resolved; however, these small oscillations are also likely to be related to the statistics of the `CGMF` calculations.

In addition to that, structures that reflect the physics, like the opening of second-chance fission (around 6 MeV for both, ^{235}U and ^{239}Pu) and the pre-equilibrium peak, are not fully reproduced by `CGMF`. For instance, the ^{235,238}U PFNS show around second-chance fission a sharp triangular structure from 200–800 keV outgoing-neutron energy. While experimental data support a structure there, it is distinctly less pronounced and not that sharp. The magnitude of the structure can be changed by tweaking the multiple-chance fission probabilities. If, for instance, the fission probabilities of Ref. [4] are used compared to the initial parameters of $\texttt{CoH}_3$, the structure lessens in magnitude and agrees slightly better with experimental data in Fig. 17. However, the triangular shape is still too pronounced and the PFNS is overall too soft. At least for ^{235}U(n,f), the experimental data from Chi-Nu is given for large incident-energy bins covering about 1 MeV. Averaging the `CGMF` calculations with the experimental neutron flux over this energy range could soften the sharp triangular shape seen at $E_{\rm inc} = 6.5$ MeV. This needs to be further explored. Tweaking the $\langle$TKE$\rangle$ does little to improving the agreement with experimental data; however, preliminary studies show that large change in the spin cut-off parameter lead to a harder spectrum, at the cost of increasing the average γ-ray multiplicity. Further studies are needed to resolve these issues. Beneficially, since `CGMF` records the energies of all of the emitted neutrons—and whether they are emitted from the fission fragments or the compound before fission—we can determine which part, or parts, of the model should be investigated further.

The systematically too soft `CGMF` PFNS can also be observed in the mean energies of ^{235,238}U and ^{239}Pu in Figs. 9–11 that were calculated from the PFNS. The mean energies are—with few exceptions—systematically too low compared to evaluated mean energies. However, the location of first- and second-chance fission seems to agree with that predicted by evaluations. The overall shape of the mean energy of ^{239}Pu seems to agree with ENDF/B-VIII.0. This observation seems to indicate that a

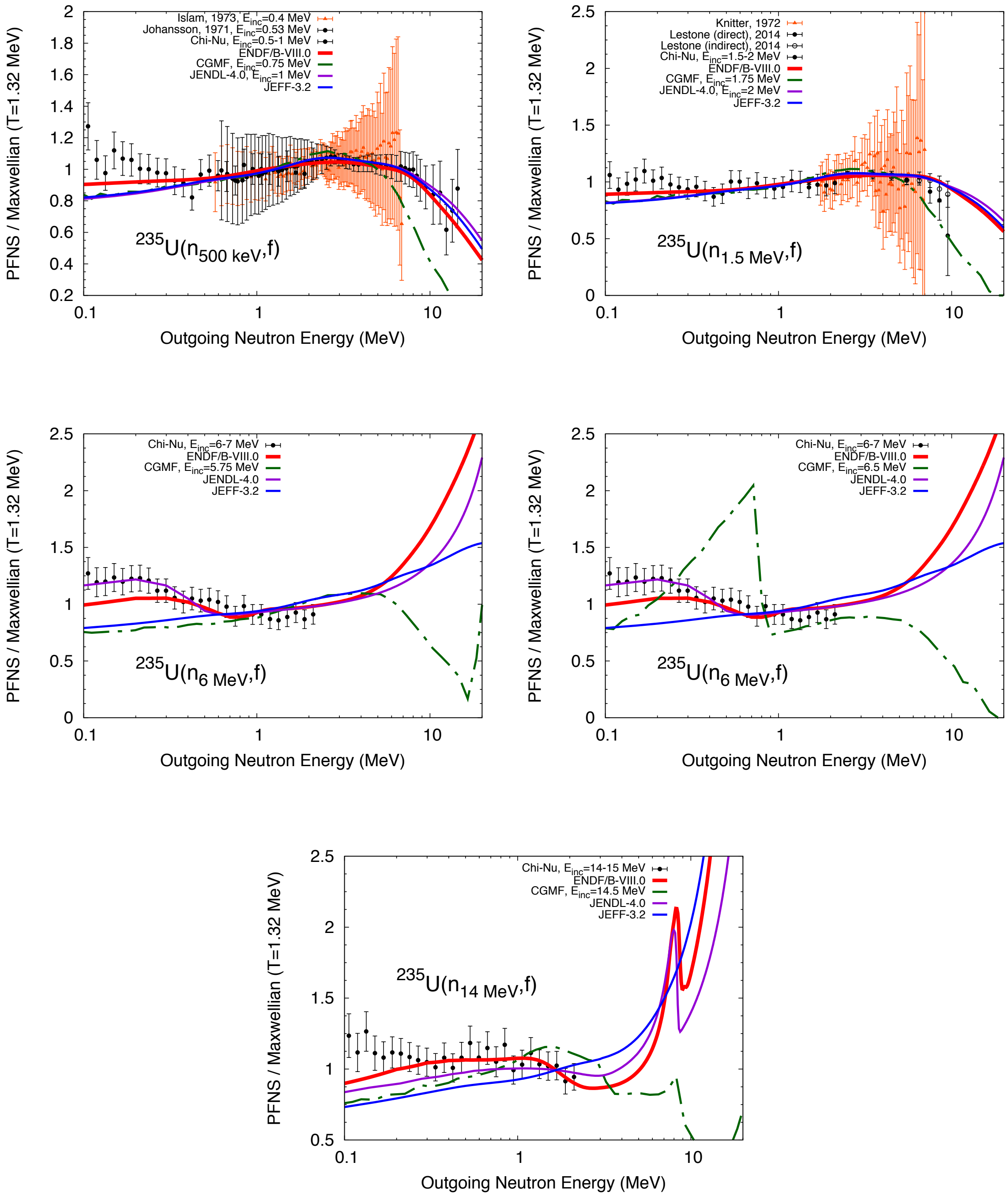

Figure 12: The ^{235}U CGMF PFNS are compared to ENDF/B-VIII.0, JENDL-4.0, JEFF-3.2 and experimental data used for the ENDF/B-VIII.0 evaluation.

scaling of the PFNS to harden the spectrum could solve the PFNS `CGMF` issue. However, it is obvious that the shapes of ^{235,238}U mean energies do not agree with current evaluated data. Hence, a global scaling factor for all PFNS might be out of reach.

In summary, we would caution against using the `CGMF` PFNS model calculations in their present form and using initial model-parameter sets for evaluation purposes. Even, if they are used as a non-informative prior with adequate experimental data, one would still need a reliable model that allows for extrapolation of PFNS to E_{inc} and E without experimental data. This reliability of `CGMF`-predicted

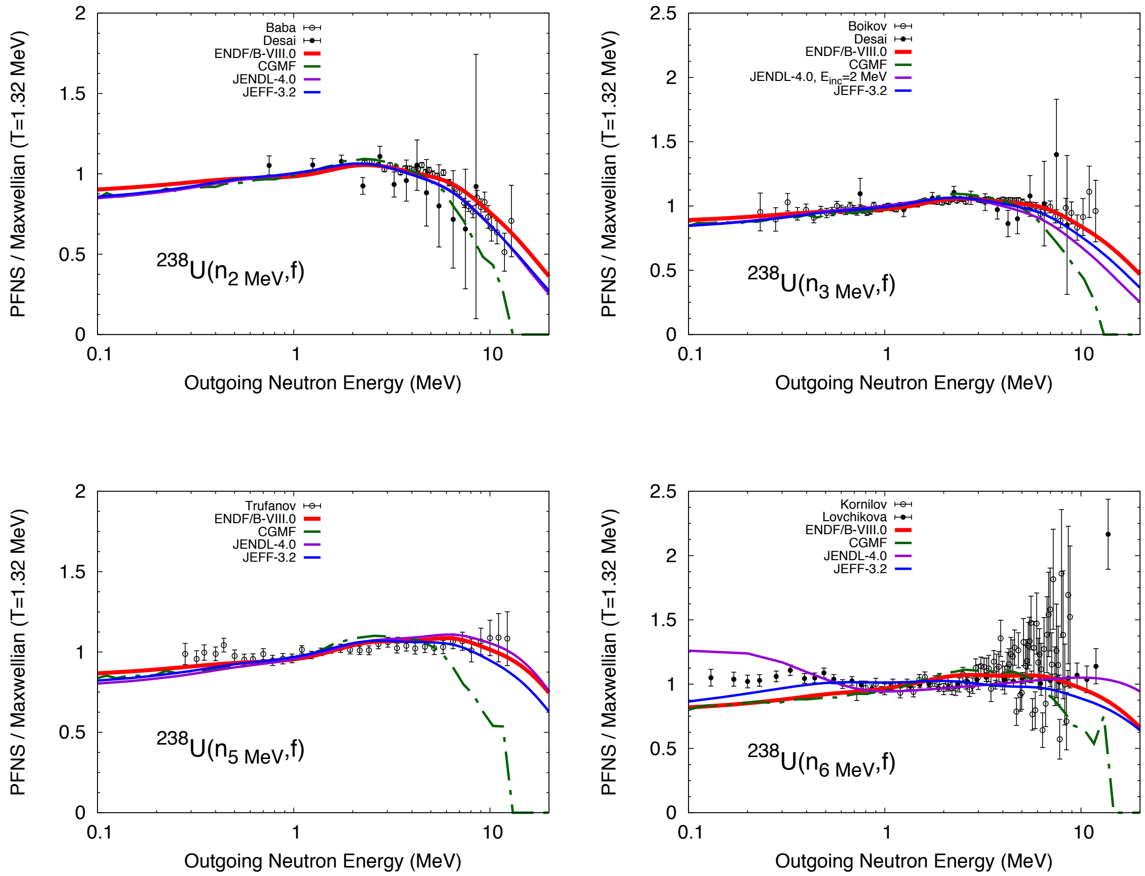

Figure 13: The ^{238}U CGMF PFNS are compared to ENDF/B-VIII.0, JENDL-4.0, JEFF-3.2 and experimental data used for the ENDF/B-VIII.0 evaluation.

PFNS is currently not guaranteed. Even if Gaussian Processes are used to mitigate the shortcomings in the model, this is not recommended as the model curves are too far away from experimental data. Hence, in energy ranges without experimental data, the Gaussian Processes would default (after a transition region) back to model values which are in their present form too biased for evaluation purposes. However, initial studies on changes in model parameters and improvements of the model showed that the `CGMF` PFNS can be improved. Further investigations—either in the direction of accounting for model defects or removing biases in the model description of the PFNS—are needed before using `CGMF` for PFNS evaluations.

The $\overline{\nu}$ of `CGMF`, however, describes existing experimental data well for ^{235,238}U and ^{239}Pu in Figs. 18–21. The thermal $\overline{\nu}$ values of ^{235}U(n,f) and ^{239}Pu(n,f) agree very well with both experimental and evaluated data within their respective uncertainties in Fig. 18. Given that ENDF/B-VIII.0 is based on a detailed analysis of existing experimental data, it is easy to understand that ENDF/B-VIII.0 agrees well with the data. `CGMF` parameters, on the other hand, were fitted to reproduce experimental data, and the model is able to reproduce them. The discrepancy between the thermal values of ^{238}U(n,f) $\overline{\nu}$ from ENDF/B-VIII.0 and `CGMF` is not indicative of a shortcoming in `CGMF` given that no experimental data exist for this sub-fission-threshold value to validate one calculated value over the other.

The `CGMF`-calculated ^{235}U(n,f) $\overline{\nu}$ values are well within the spread of existing experimental data in Fig. 19. They seem a bit low compared to experimental data for 0.15–1.5 MeV. The `CGMF`-calculated ^{235}U(n,f) $\overline{\nu}$ values are rarely within the 1-σ uncertainties of ENDF/B-VIII.0. That issue can be

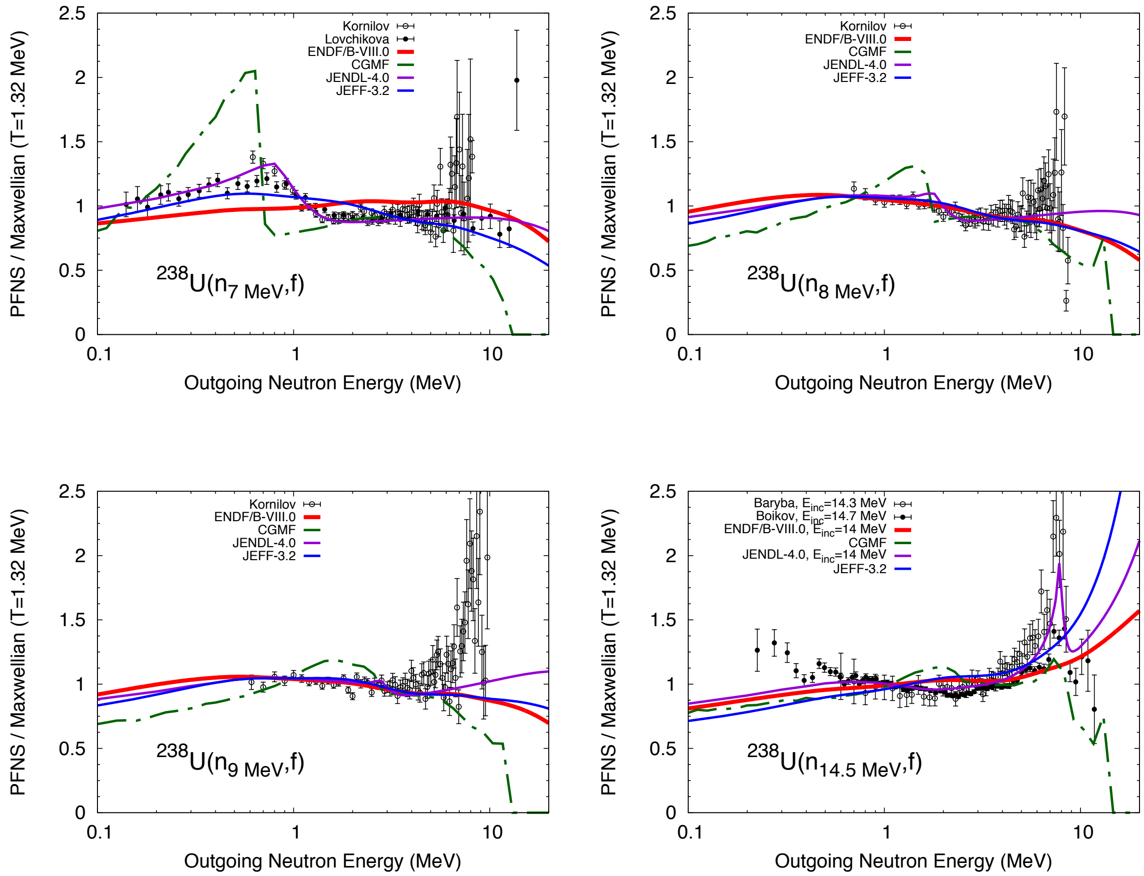

Figure 14: The ^{238}U CGMF PFNS are compared to ENDF/B-VIII.0, JENDL-4.0, JEFF-3.2 and experimental data used for the ENDF/B-VIII.0 evaluation.

partially attributed to unrealistically low ENDF/B-VIII.0 uncertainties; they are significantly lower than the standard (^{252}Cf(sf) $\overline{\nu}_{\rm tot}$). Changing the $\langle$TKE$\rangle$ within a physically-defined space (*i.e.*, by the spread in experimental data) would be able to increase the $\overline{\nu}$ between 0.14–1.5 MeV for ^{235}U such that it agrees with experimental data all the while the mean energy of the PFNS is impacted less significantly as can be seen in Fig. 8.

The structures in ^{235}U(n,f) $\overline{\nu}$ values of `CGMF` around second- and third-chance fission are also interesting to note. Experimental data would not completely exclude structures there but would indicate less pronounced ones. If the multiple-chance fission probabilities of Ref. [4] are used, the $\overline{\nu}$ of ^{235}U shows less pronounced structures around second- and third-chance fission in Fig. 8, while the PFNS mean energy also become more reasonable. Hence, fixing the structures in and too low $\overline{\nu}$ of ^{235}U seems attainable with optimizing the parameters of `CGMF`.

For ^{238}U(n,f) $\overline{\nu}$, `CGMF` agrees mostly with experimental data and with evaluated data within their uncertainties above the fission threshold. However, it does not predict the slope change of the evaluated data around approximately 3 MeV in Fig. 20 that is seemingly visible in experimental data. It is unclear if that is an an experimental artifact or real physics. Vibrational states could be a reason for the slope change but `CGMF` does not model them. In addition to that, the second-chance fission structure around 6 MeV is not at all observed in experimental data. This shortcoming can be fixed by improving multiple-chance fission probabilities to change more gradually with incident-neutron energy as shown for ^{235}U, as well as in smoothing out the sudden jump in $\langle$TKE$\rangle$ that is seen in Fig. 3 for ^{238}U as well

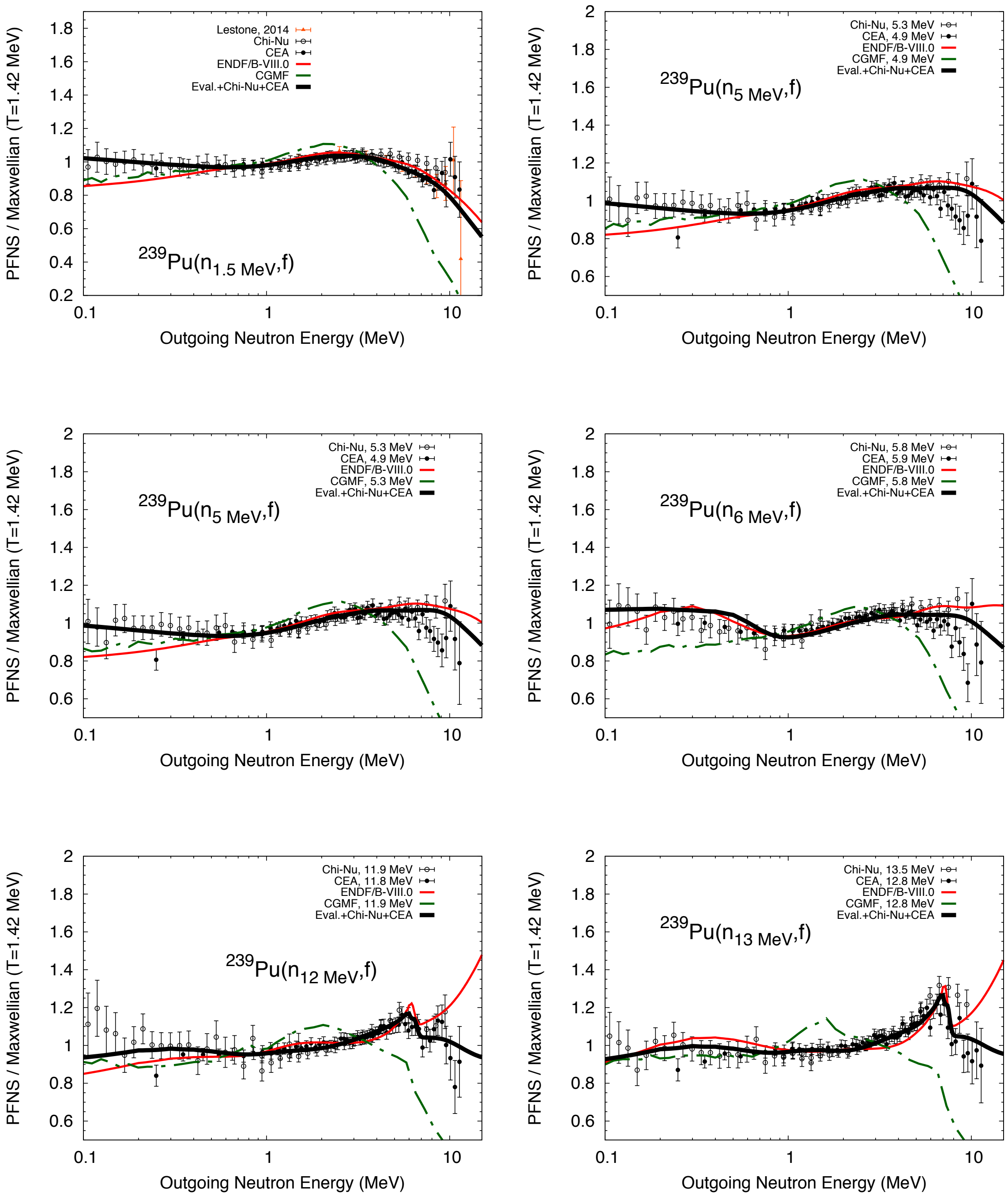

Figure 15: The ^{239}Pu CGMF PFNS are compared to ENDF/B-VIII.0, a recent evaluation using CEA and Chi-Nu experimental data by D. Neudecker and Chi-Nu and CEA experimetnal data.

as for ^{235}U.

The ^{239}Pu(n,f) $\overline{\nu}$ predicted by `CGMF` agree overall well with existing experimental data. Although, they are slightly outside of the range of 1-σ ENDF/B-VIII.0 evaluated uncertainties in Fig. 22. However, recent work by D. Neudecker using the "Physical Uncertainty Boundary" (PUB) method by Vaughan *et al.* indicate that these uncertainties are underestimated [65, 66]. If CGMF-predicted values of ^{239}Pu(n,f) $\overline{\nu}$ are compared to PUB's bounds (see Fig. 22), it is obvious that `CGMF` is able to predict realistic ^{239}Pu(n,f) $\overline{\nu}$ given existing experimental data.

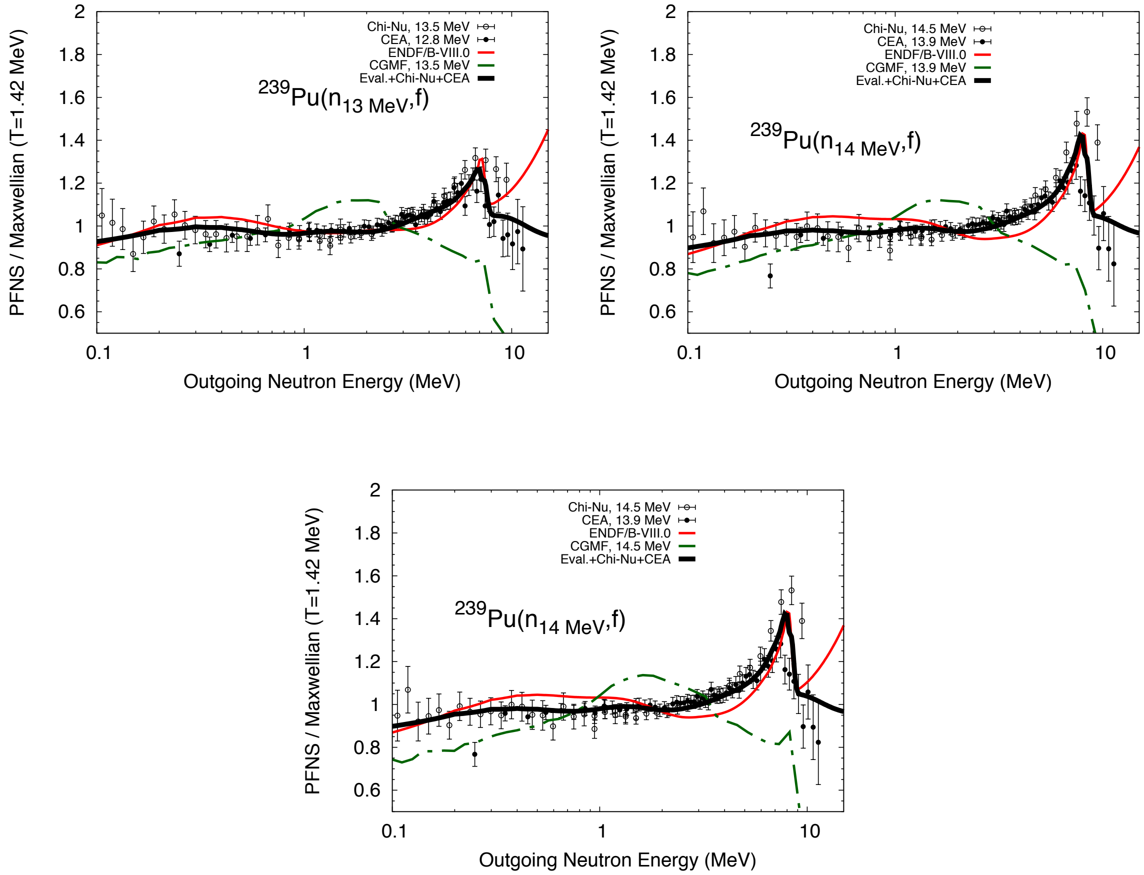

Figure 16: The ^{239}Pu CGMF PFNS are compared to ENDF/B-VIII.0, a recent evaluation using CEA and Chi-Nu experimental data by D. Neudecker and Chi-Nu and CEA experimetnal data.

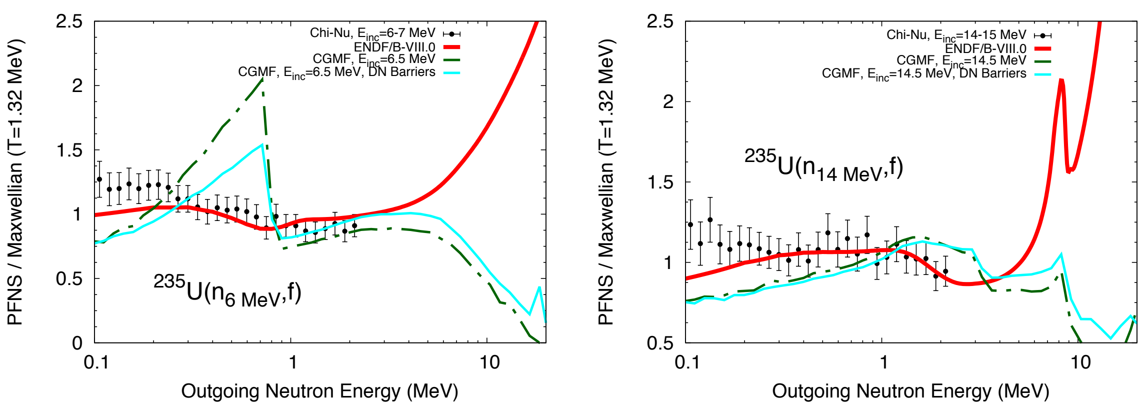

Figure 17: The ^{235}U CGMF PFNS at incident-neutron energies of 6.5 and 14 MeV using default and fission-barrier parameters of Ref. [4] are compared to ENDF/B-VIII.0 and experimental data used for the ENDF/B-VIII.0 evaluation. While using the fission-barrier parameters of Ref. [4] improves the agreement with experimental data, the `CGMF` PFNS still distinctly differs from them.

In short, `CGMF` could possibly be used to evaluate $\overline{\nu}$. To this end, the model parameters of `CGMF`, especially the multiple-chance fission probabilities and $\langle$TKE$\rangle$ should be tuned to better reproduce experimental data of ^{235,238}U(n,f) $\overline{\nu}$ close to the second- and third-chance fission threshold. For ^{238}U(n,f)

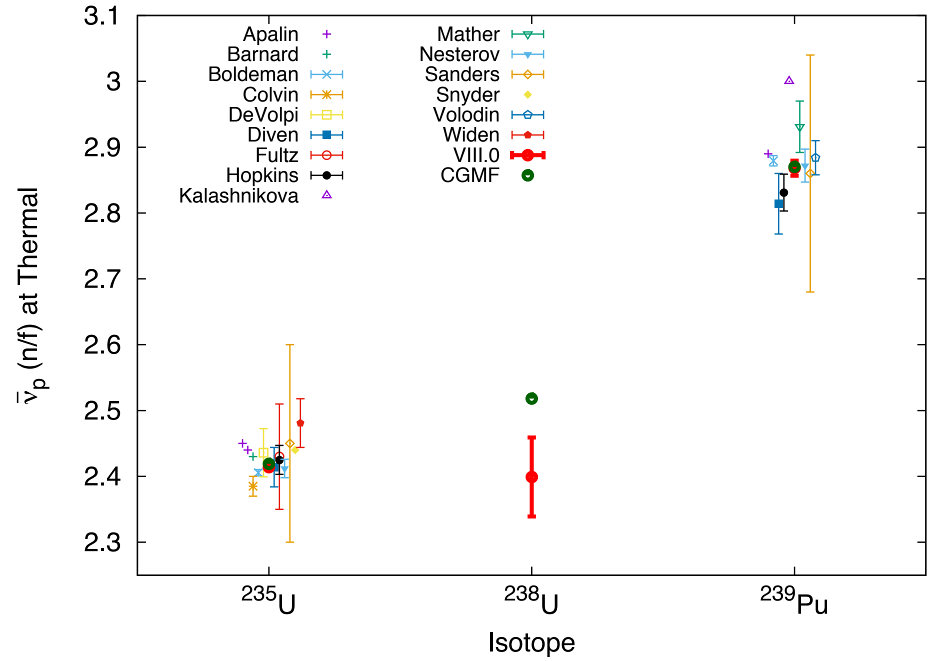

Figure 18: The thermal ^{235,238}U and ^{239}Pu $\overline{\nu}$ CGMF-calculated values are compared to experimental data and ENDF/B-VIII.0 nuclear data.

$\overline{\nu}$, it should also be investigated whether the slope change at 3 MeV is physically justifiable or a measurement artifact. (Preliminary studies with `CGMF` show that a flattening of $\overline{\nu}$ at low incident energies is caused by the slope change of $\langle \mathrm{TKE} \rangle$ in Eq. (9).) However, even if `CGMF` can be used to evaluate $\overline{\nu}$, the remaining challenge is that we cannot use it for PFNS evaluations—at least not with the initial parameter values. As mentioned above, a small change in parameters to better fit PFNS entails an even larger change for $\overline{\nu}$, and for parameters, where large changes can harden the tail of the PFNS, these changes come at the cost of reliably predicting some γ observables. However, initial studies here indicate that changes in the parameters to fix one of the two observables, leads to improvements in the other. Further studies are needed how to solve this issue; some additional investigations in this matter are given below.

During the summer of 2019 and 2020, two pairs of summer students from the "XCP Computational Workshop" worked with A.E. Lovell, I. Stetcu, and P. Talou on two separate projects trying to address the discrepancy between the PFNS calculated with `CGMF` and experimental data. In the first project, physics models were explored to try to reduce this discrepancy, and in the second, an emulator was constructed to take into account this discrepancy.

In 2019, C. Parker and S. Pineda studied the effects of the optical potential—the effective interaction between a heavy target and light projectile—on the PFNS. Most global optical potentials, *e.g.* [7–9], are parametrized as a function of mass, charge, and incident-particle energy and have been fit to scattering data such as elastic-scattering angular distributions, polarization observables, and total/ reaction cross sections for stable targets or targets near stability. Each optical potential typically uses a different subset of reaction data in the optimization, as well as a different parametrization. There are also known to be compensating effects between optical model parametrizations, where two different parametrizations can lead to the same elastic-scattering observables. In addition, because the potentials are constrained near stability, beyond this region, they rely on extrapolations, which can be of varying quality. These potentials are needed in the Hauser-Feshbach formalism for fission to calculate the probability of neutron emission at a given energy from the fission fragments—nuclei

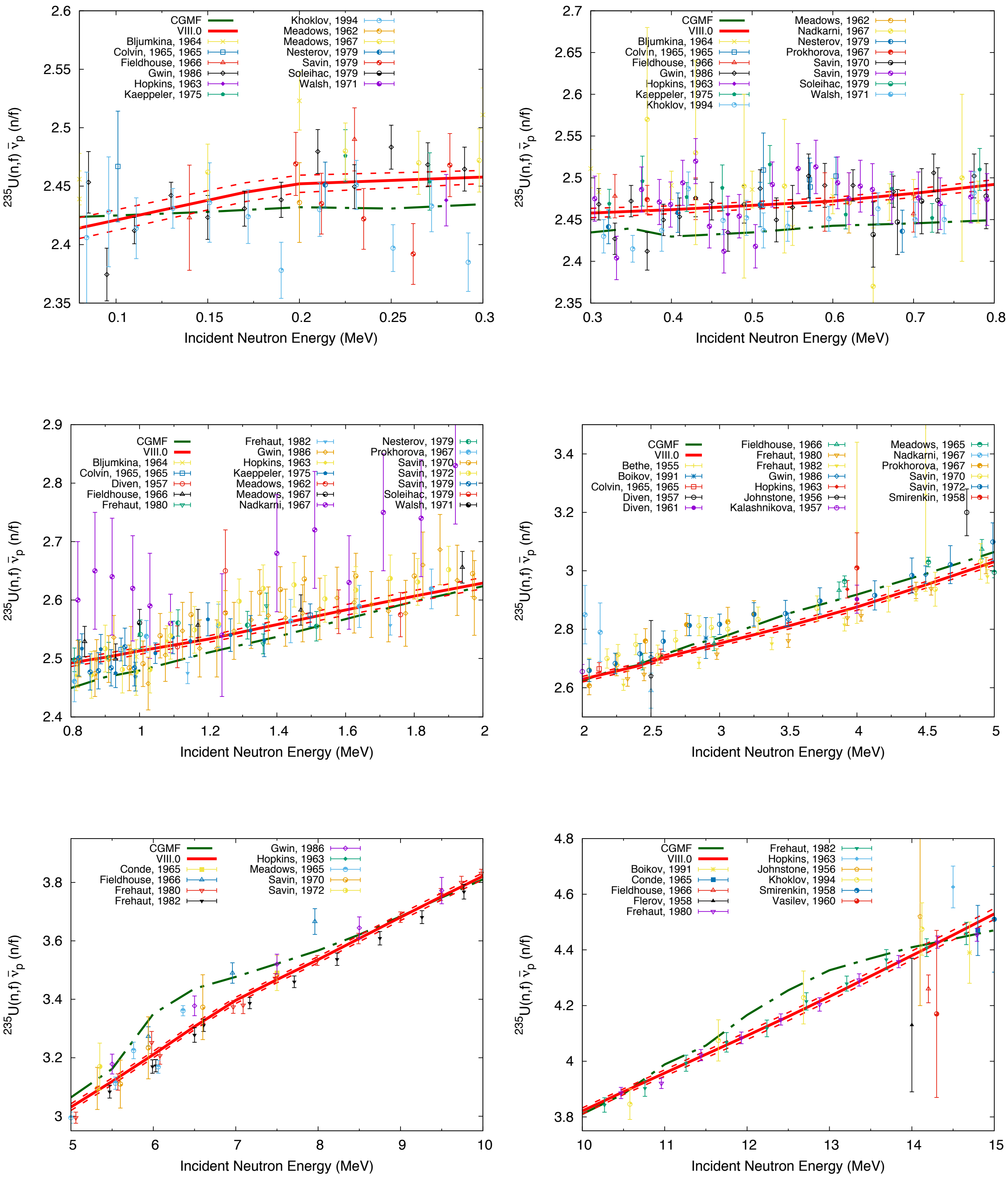

Figure 19: The ^{235}U $\overline{\nu}$ CGMF-calculated values are compared to experimental data and ENDF/B-VIII.0 nuclear data. Each plot zooms into a specific energy range for increased visibility.

that are much further from stability than the targets used to constrain the potentials. Additionally, because there is still limited to no experimental data (*e.g.*, cross sections) in these regions, it is difficult to assess the quality of the extrapolations.

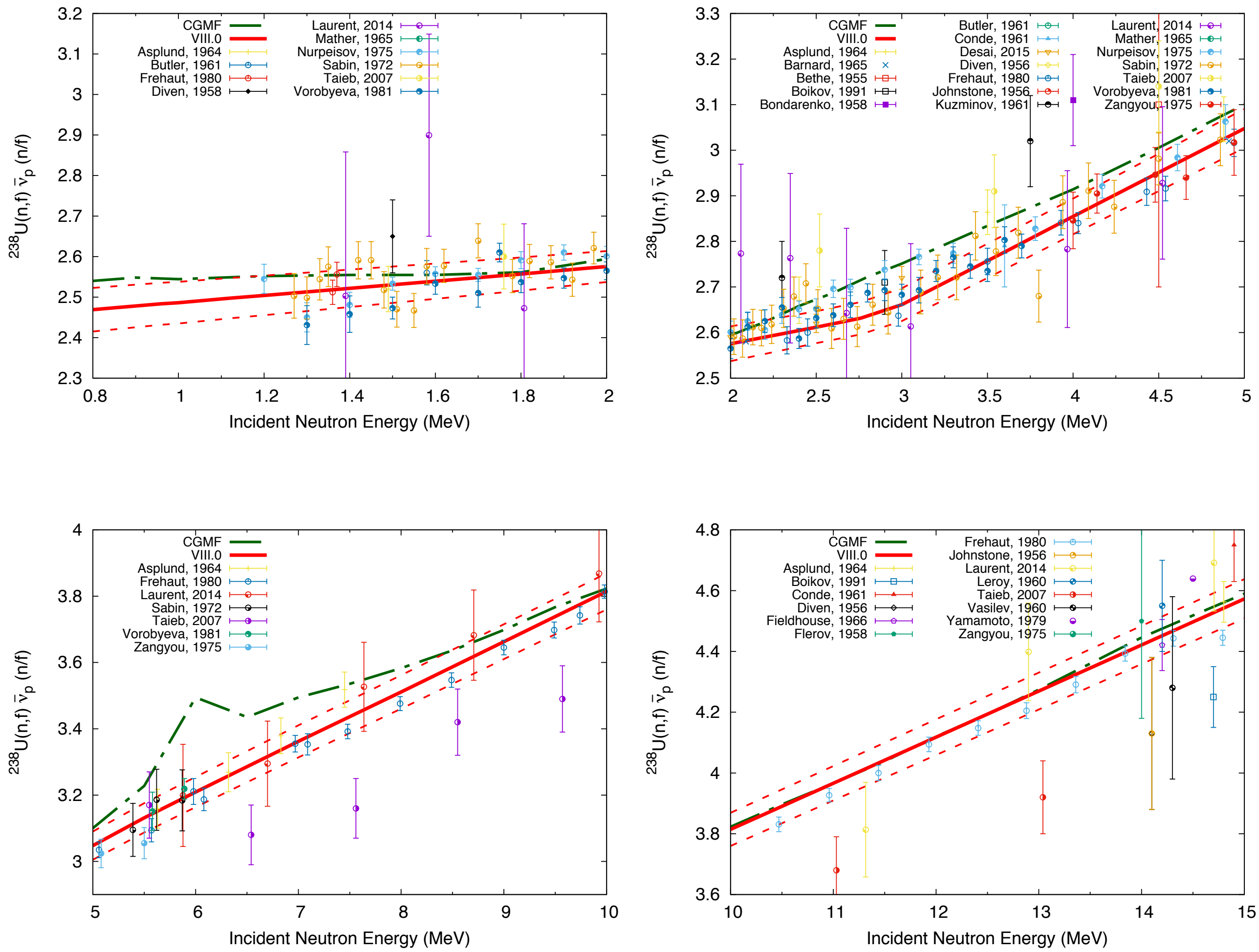

Figure 20: The ^{238}U $\bar{\nu}$ CGMF-calculated values are compared to experimental data and ENDF/B-VIII.0 nuclear data. Each plot zooms into a specific energy range for increased visibility.

C. Parker and S. Pineda explored several different optical potentials [7–9], calculating the χ^2 per degree of freedom of the total cross section calculated with these potentials to the available experimental data. Then, they used CoH$_3$ to construct an approximate PFNS from the calculated neutron spectra at incident energies equating to excitation energies in the compound

$$\chi(\varepsilon_i) = \sum_{A,Z} Y(A,Z) \sum_{E_i} f(E_i+6)\chi(\varepsilon_i|A-1,Z,E_i), \tag{18}$$

where $\chi(\varepsilon_i|A,Z,E_i)$ is the neutron spectrum for a fission fragment (A,Z) (not, the $A-1$, due to the spectrum being calculated for a neutron-induced reaction), $Y(A,Z)$ is the mass and charge distribution of the fission reaction, and $f(E_i)$ is a weighting function to take into account the distribution of excitation energies within the fission fragments. Here, we add $\sim$ 6 MeV to E_i in this distribution to account for the energy difference between the incident energy used in CoH$_3$ and the excitation energy of the fission fragment, which is approximately the neutron-separation energy for each fragment. Even with a relatively light computational code such as CoH$_3$, performing this sum over roughly 40 excitation energies for at least a hundred nuclei is time consuming. Therefore, the students also made an approximation similar to a Los Alamos model-like (LAM) PFNS [69] by including in Eq. (18) only the two most abundant isotopes—those in the light and heavy peaks. In the center-of-mass frame of the fission fragments, this results in a decrease of the mean energy of the PFNS by about 50 keV.

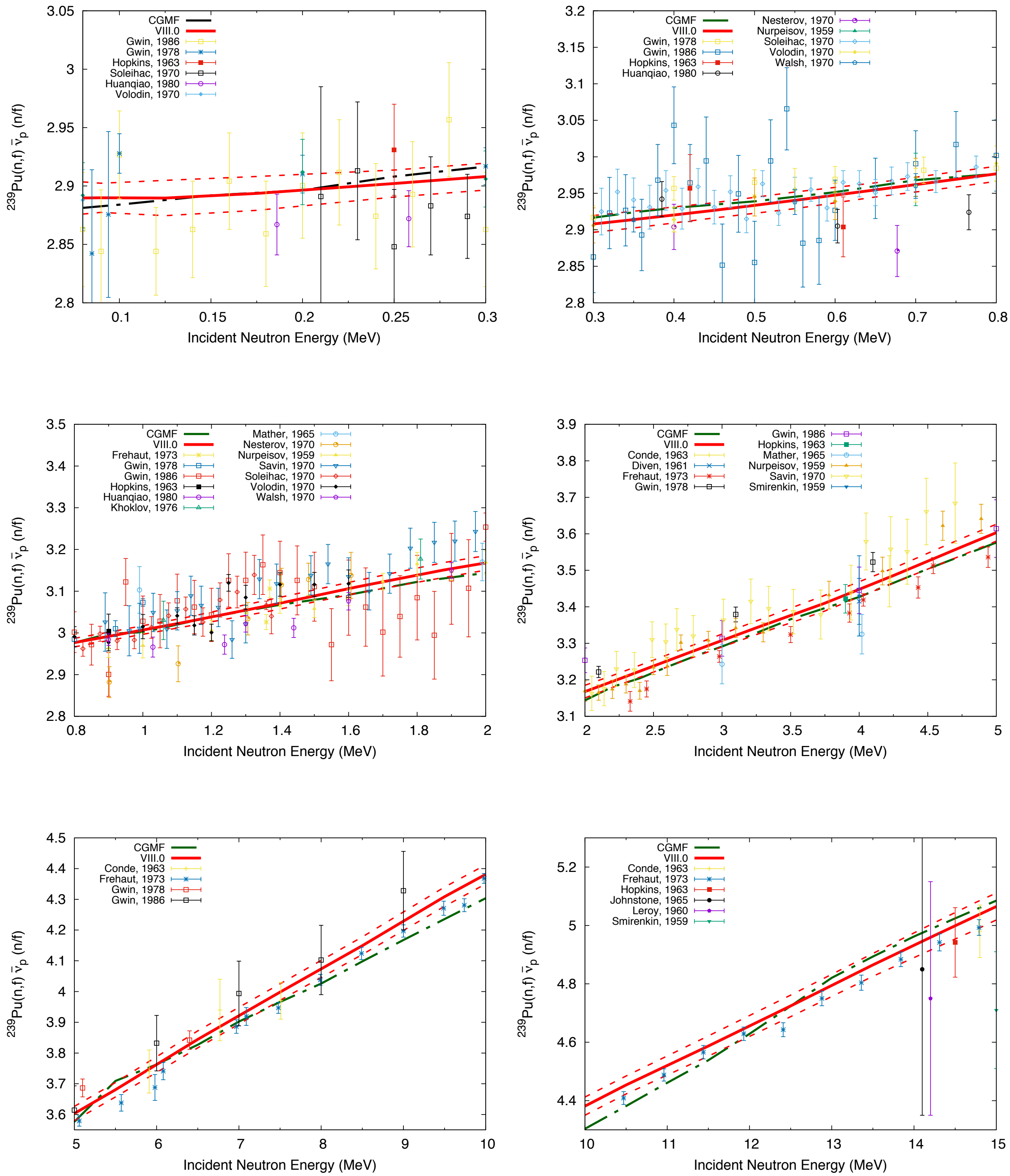

Figure 21: The ^{239}Pu $\overline{\nu}$ CGMF-calculated values are compared to experimental data and ENDF/B-VIII.0 nuclear data (including 1-σ uncertainties). Each plot zooms into a specific energy range for increased visibility.

We continued these studies FY20 with the understanding that most optical potentials are constrained with data close to the stable nuclei. Hence, we explored for ^{252}Cf(sf) optimizing the optical-

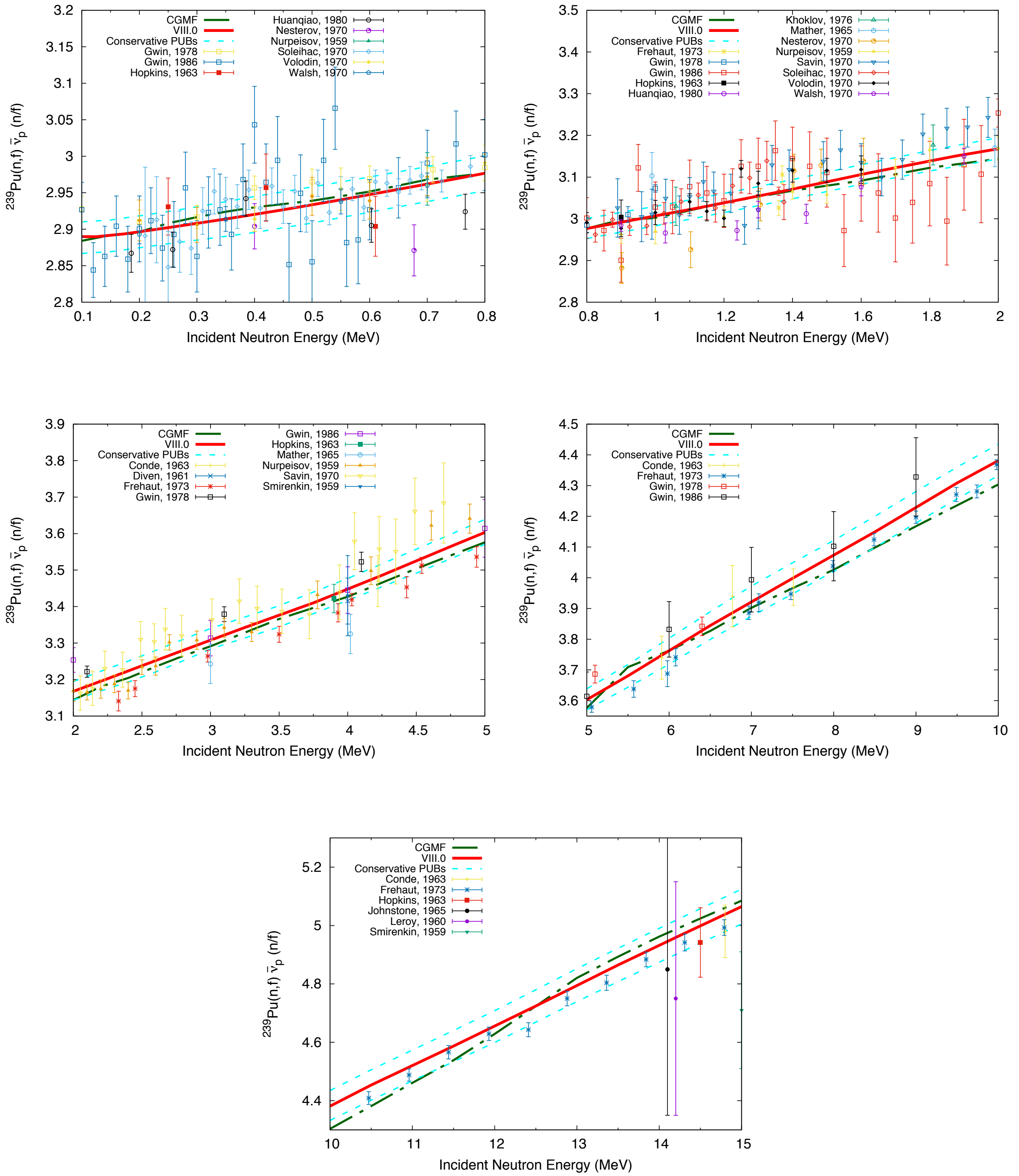

Figure 22: The ^{239}Pu $\overline{\nu}$ CGMF-calculated values are compared to experimental data and ENDF/B-VIII.0 nuclear data. Conservative 1-σ PUBs bounds indicate that CGMF predicts ^{239}Pu $\overline{\nu}_p$ in reasonably. Each plot zooms into a specific energy range for increased visibility.

model parameters with respect to the most exotic (*e.g.*, far from stability), experimentally measured nuclei in the isotopic chains containing the peaks of the yield distribution, ^{99}Tc and ^{133}Cs. The peaks of the yield distribution in `CGMF` are ^{110}Tc and ^{142}Cs. Hence, these nuclei are both about 10 neutrons

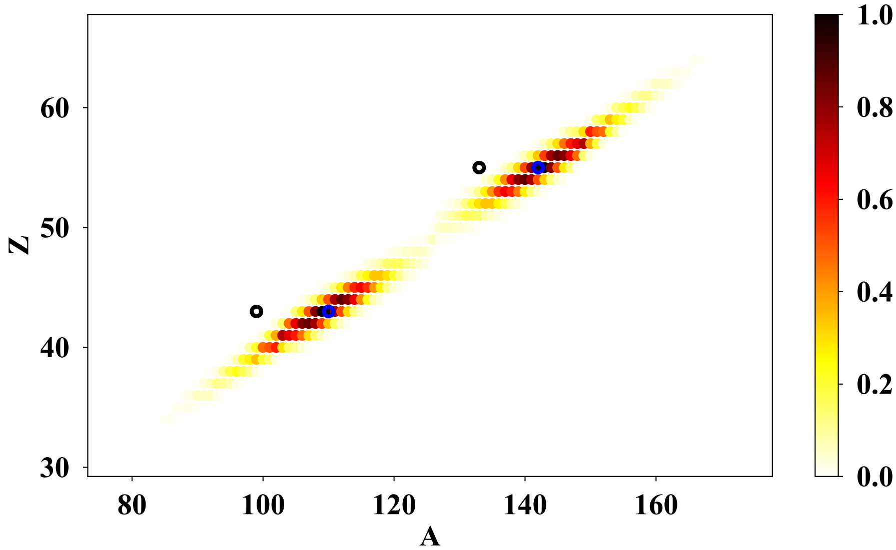

Figure 23: Yields as a function of mass and charge for ^{252}Cf(sf). Blue circles highlight the heavy and light peaks. Black circles indicate the nuclei in those two isotopic chains where the total cross section has been experimentally measured.

away from the peaks in the distribution, illustrated in Fig. 23. Still, we found that by fitting the optical-model parameters to these data sets, the result on the LAM PFNS was an increase of mean energy of the PFNS by ~ 20 keV in the center-of-mass frame of the fission fragments, shown in Fig. 24. This increase in mean energy was calculated by scaling the depth radius and diffuseness of the ^{99}Tc+n and ^{133}Cs+n optical potential parameters, not taking into account any potential change in the energy dependence of the optical potential or difference between mass and charge. Further studies are underway to explore possible updates of the optical-model parameters as a function of mass and charge, by looking across well-measured isotopic chains. While the 20 keV increase found in this small study is promising, the mean energy for ^{252}Cf(sf) from `CGMF` is about 150 keV lower than those derived from experimental PFNS, and 20 keV only represents a small part of the needed change. However, we have seen earlier in this section that mean energies of some isotopes are closer to experimental data than others, possibly indicating that certain neutron-target interactions need more of a tweak than others; this hypothesis would need to be investigated in more detail, and further studies are underway.

During the summer of 2020, A.E. Lovell and I. Stetcu, with the help of M.J. Grosskopf, again had two students through the XCP Computational Workshop, S. Blade and S. Ozier, who trained an emulator to model the discrepancy between `CGMF` and experimental data, beginning with the mean energies of the PFNS. Emulators will be described in more detail in Section 6, but the main idea is to have a function that corrects the code results based on experimental data. Currently, preliminary results have been produced and are shown in Fig. 25 for both ^{239}Pu(n,f) (left) and ^{235}U(n,f) (right) compared to data taken by the Chi-Nu group (provided by K.J. Kelly) [5]. The emulator is able to correct both the magnitude and shape of the `CGMF` calculations. However, the emulator appears to have more difficulty training on the discrepancy between theory and data for ^{235}U(n,f), where the differences are less consistent–which may led to the large uncertainties between the experimental data points in Fig. 25 (left), compared to the relatively constant emulator uncertainties for ^{239}Pu (right). Further studies are underway to understand these differences between the two reactions, as well as to test the covariance function within the emulator, its predictive power, as well as the impact of the spread in the incident energy of the model calculations.

With the sensitivity studies shown in Section 3, a Gaussian Process emulator could also be used to

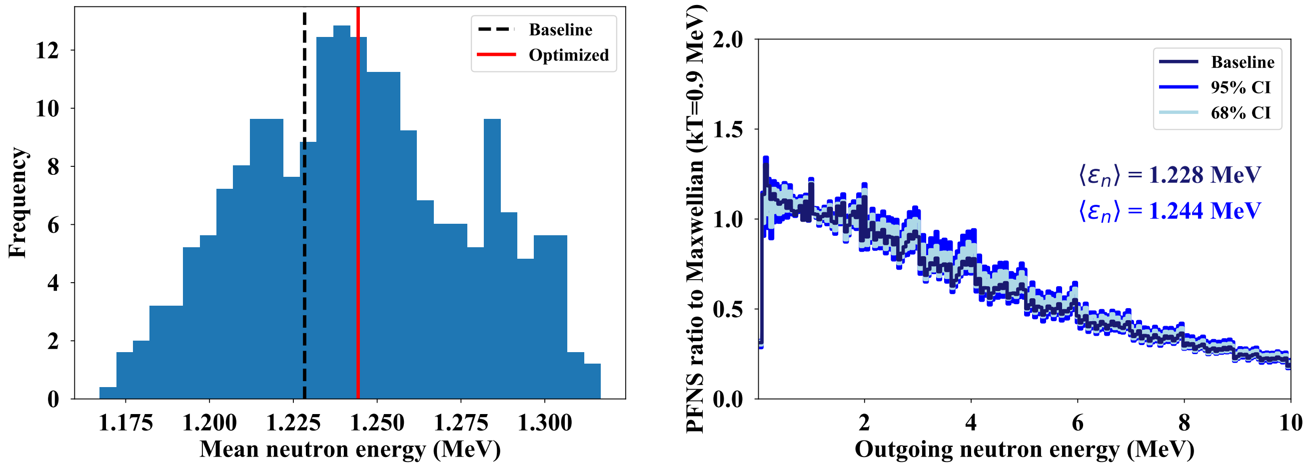

Figure 24: (Left) Distribution of mean neutron energies from the LAM PFNS (shown right) resulting from the optimization of the optical potentials of ^{99}Tc+n and ^{133}Cs+n. Black dashed line shows the mean energy before the optimization and the red solid line shows the average across the plotted histogram. (Right) PFNS as a ratio to Maxwellian (kT=0.9 MeV) resulting from the OMP optimization. The PFNS before optimization is shown in dark blue, while the blue (light blue) regions give the 95% (68%) confidence intervals resulting from the optimization.

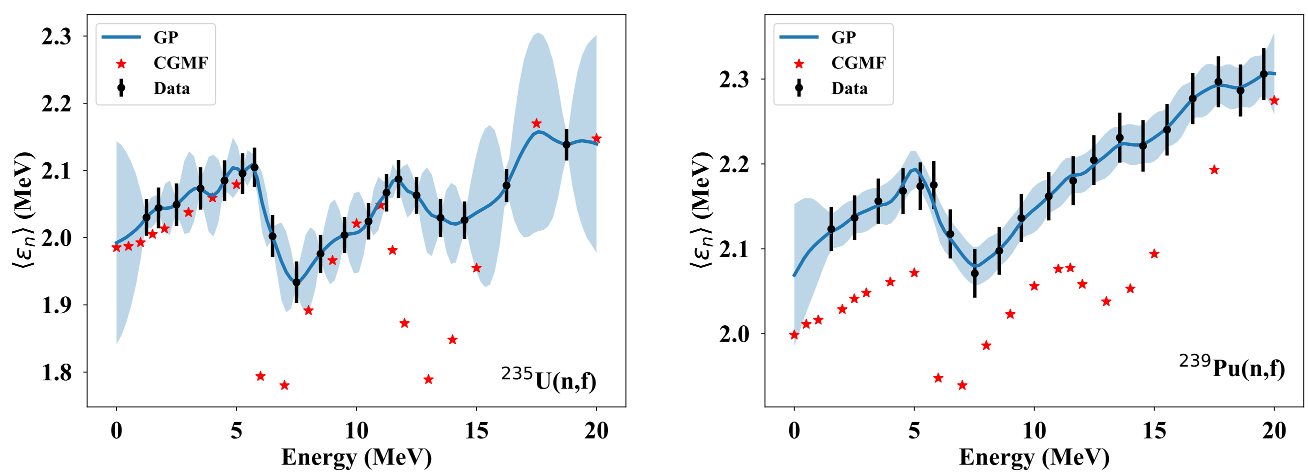

Figure 25: Preliminary results from the emulator modeling the discrepancy between `CGMF` calculations for the mean energy of the PFNS and experimental data from Chi-Nu for (left) ^{239}Pu(n,f) and (right) ^{235}U(n,f).

further optimize those parameters that are found to be sensitive to the average number of neutrons, mean energy, and PFNS. For example, as we have seen that the total kinetic energy parametrization and the multi-chance fission probabilities can change $\overline{\nu}$ and the average neutron energies, we can train an emulator on variations in just these model parameters and further optimize the output of `CGMF` without requiring thousands of full model runs.

In addition, `CGMF` has already been shown to make good predictions for the average γ multiplicity, N_γ, and accurately produces the prompt fission γ-ray spectrum, PFGS, based on experimentally measured γ levels, as from RIPL [3, 67, 68]. Therefore, this same method for consistent evaluations could be used to evaluate N_γ and the PFGS simultaneously. Many of these mitigation strategies would also not be needed in this case, as the γ-ray observables are already well-reproduced by `CGMF`.

6 Evaluation Techniques

For the recent ENDF/B-VIII.0 ^{235}U and ^{239}Pu evaluated PFNS, $\boldsymbol{\psi}$, and associated covariances, $\mathbf{Cov}^{\psi}$, were obtained by a generalized least squares algorithm [4] (GLS) including model data, $\boldsymbol{\chi}$, and covariances, $\mathbf{Cov}^{\chi}$, and experimental data, $\boldsymbol{N}$, and covariances $\mathbf{Cov}^{N}$, by:

$$\begin{aligned}\boldsymbol{\psi} &= \boldsymbol{\chi} + \mathbf{Cov}^{\psi}\boldsymbol{S}^t(\mathbf{Cov}^{N})^{-1}\left(\boldsymbol{N} - \boldsymbol{S}\boldsymbol{\chi}\right),\\ \mathbf{Cov}^{\psi} &= \mathbf{Cov}^{\chi} - \mathbf{Cov}^{\chi}\boldsymbol{S}^t Q^{-1}\boldsymbol{S}\mathbf{Cov}^{\chi},\end{aligned} \tag{19}$$

where

$$Q = \boldsymbol{S}\mathbf{Cov}^{\chi}\boldsymbol{S}^t + \mathbf{Cov}^{N}. \tag{20}$$

To this end, $\boldsymbol{N}$ at a specific E_{inc} must be rescaled with one multiplicative factor with respect to the model data. This scaling factor was calculated by taking the ratio of numerical integrals of $\boldsymbol{\chi}$ and $\boldsymbol{N}$ at the same or the nearest E_{inc} for the same outgoing neutron energy range.

The design matrix $\boldsymbol{S}$ and its transpose $\boldsymbol{S}^t$ were calculated in Ref. [4] by linear interpolation to bring experimental data onto the E_{inc} and E grid of the prior (model) data. Here, a different approach to calculate $\boldsymbol{S}$ is taken that transforms GLS into the Kalman filter technique. Contrary to Ref. [4], $\boldsymbol{\chi}$ are model-parameter values and $\mathbf{Cov}^{\chi}$ are their covariances. We only update those model parameters that the PFNS and $\overline{\nu}$ are sensitive to.

The design matrix needs to convert experimental data into model-parameter space. This is achieved by taking as $\boldsymbol{S}$ the sensitivity vectors R_{ij} as discussed in Section 3. This different approach is taken here because `CGMF` PFNS and $\overline{\nu}$ calculations are computationally expensive. The LAM used in Ref. [4] was much faster and allowed to calculate thousands of model-calculated PFNS for equally many parameter sets that could then be used for estimating $\mathbf{Cov}^{\chi}$ in PFNS space. This is prohibitively expensive for `CGMF` and therefore the Kalman-filter technique, which requires only calculating the sensitivities of the most important parameter in a few dozen runs, is more desirable. Hence, the resulting $\boldsymbol{\psi}$ are actually `CGMF` model parameters that can then be applied to obtain evaluated data. If Gaussian Processes (GP) are used to account for model defects in PFNS calculations, the GP parameters will become part of $\boldsymbol{\chi}$ and, hence, the updated $\boldsymbol{\psi}$.

A Gaussian process is a non-parametric model that aims to find a distribution over all possible functions that are consistent with the data [70]. The GP is defined by a mean, $m(\mathbf{x})$, and a covariance function, $k(\mathbf{x}, \mathbf{x}')$,

$$f(\mathbf{x}) \sim \mathcal{GP}(m(\mathbf{x}), k(\mathbf{x}, \mathbf{x}')). \tag{21}$$

In most applications, the mean function is taken to be zero, and the covariance function can have many forms but is defined by a strength and a correlation length. The strength and correlation length are determined by tuning to a set of training data, and then predictions outside of the training data can be made. Predictions that are between training points are typically more accurate than predictions beyond the training set, because outside of the bounds of the training set, the GP goes back to the mean function beyond one or two correlation lengths.

Gaussian processes are commonly used in two ways, as mentioned above to account for model defects and as emulators to speed up calculations (typically for parameter optimization). While the preliminary studies into discrepancy modeling, shown in Section 5, appear to be able to correct `CGMF` calculations to experimental data (albeit, with some overfitting that needs to be addressed), more in depth studies need to be performed to understand the challenges that could arise for a 2D emulator with discrepancy—if this path were to be used to correct the PFNS from `CGMF` to experimental data—and to quantify the quality of the emulator for interpolation and extrapolation. Using the emulator in this manner would also somewhat decouple the final PFNS evaluation from the underlying physics within `CGMF`.

Instead, using the GP to speed up the `CGMF` calculations for parameter optimization would keep the connection to the underlying physics and make optimization of the underlying parameters more feasible. Still, further studies have to be performed to pin down the models within `CGMF` that can change the shape of the PFNS along with the mean neutron energy.

7 Summary

This report here was written in answer to a FY20 NCSP milestone on ^{235,238}U and ^{239}Pu that states: "finalize a report assessing our methodology to evaluate prompt fission neutron spectrum (PFNS) and multiplicity consistently". To be more specific, this milestone targeted to assess whether modern LANL fission-codes such as `CGMF` [1] or `BeoH` [64] can be used in their present version for future nuclear-data evaluations of ^{235,238}U and ^{239}Pu average prompt-neutron multiplicity, $\overline{\nu}$, and the prompt fission neutron spectrum, PFNS. To this end, we studied whether these codes are able, in principle, to provide these data up to 20 MeV (`CGMF` can, while `BeoH` currently cannot due to limitations in the modeling of multiple-chance fission processes), and whether the parameter space of these codes are able to reproduce ENDF/B-VIII.0 evaluated data of these observables. Also, the steps towards a full production-run evaluation are outlined, including a survey of all available experimental data, evaluation techniques, and mitigation strategies for shortcomings in the data.

The current calculated values of $\overline{\nu}$ from `CGMF` are close enough to experimental values that with small parameter optimizations—particularly in the multi-chance fission probabilities and total kinetic energy values—`CGMF` could be used for $\overline{\nu}$ evaluations. On the other hand, the PFNS calculated from `CGMF` is too soft, compared to experimental data, across the entire incident-neutron energy range of interest and the features associated with opening of the multi-chance fission channels are either not strong enough or enter at the wrong incident-neutron energies. The strength and on-set in incident-neutron energy of some of these features could, again, be adjusted with the multi-chance fission probabilities. However, none of the parameter studies performed here had a significant enough impact on the average prompt-neutron energy or the shape of the PFNS to give us confidence that the PFNS evaluation could be preformed with `CGMF` with the model as it currently stands.

Still, there are a few promising studies underway that could improve `CGMF` PFNS calculations to a point where it can be used as a base for reliable nuclear-data evaluations:

- Preliminary studies show that a significant increase in the spin cut-off parameter can harden the PFNS. However, this comes at the cost of the γ-ray observables, which were not shown in this study.
- We have found that by adjusting the optical-model parameters for the nuclei in the peak of the pre-neutron fission yields, $Y(A,Z)$, to total cross-section data, the average PFNS energy in the center of mass was increased. Studies are on-going to determine if changes to the optical model as a function of mass and charge could further harden the PFNS.

- Preliminary studies for the mean energy of the PFNS show that a Gaussian Process emulator modeling the discrepancy between model and experiment is able to account for these differences while providing well-quantified uncertainties. A similar approach could be used for the PFNS, where a Gaussian Process discrepancy function could be constructed on top of the `CGMF` PFNS. This approach could allow us to obtain PFNS in agreement with existing experimental data through the Gaussian Process, while obtaining $\overline{\nu}$ mainly from `CGMF` calculations and experimental data. This leads to somewhat of a disconnect for $\overline{\nu}$ and the PFNS from `CGMF` . To minimize this disconnect, we will try to improve the `CGMF` PFNS calculations by investigating the parameter space of the code further. Also, additional studies would have to be performed to understand the performance of the Gaussian Process for interpolation and extrapolation as a function of both incident-neutron energy and outgoing-neutron energy. To be clear, Gaussian Processes can only be used reliably if (a) enough experimental data exists (this is the case for ^{235}U and ^{239}Pu and will be the case for ^{238}U PFNS only after Chi-Nu delivered their data) to model the PFNS and (b) if the model is reasonably close to the experimental data to give reliable extrapolated data.

- As mentioned above, we will further explore the parameter space of `CGMF` to concurrently obtain PFNS and $\overline{\nu}$ in good agreement with experimental data. Even though we have performed here sensitivity studies to many of the parameters in the pre-neutron yield model, it may be that small changes to a single parameter are not enough to strongly change the shape of the PFNS, but changes to several parameters at the same time would have a larger effect, *e.g.*, changes to the shape of $\langle \mathrm{TKE} \rangle$ or $\sigma_{\mathrm{TKE}}(A)$, which are each determined by a handful of parameters. Likewise, the energy sharing between the light and heavy fragments has been adjusted as a function of mass to experimental data for $\overline{\nu}(A)$, and changes to any of these mass-dependent values could impact the shape of the PFNS. There are also several models within `CGMF` for which there is less data available to directly constrain them, such as the Wahl systematics for the charge distribution or the energy spectra of the pre-fission neutrons. Further studies should be performed to determine how much affect each of these models had on the PFNS.

In the event that none of the above model adjustments is enough to bring the PFNS from `CGMF` in line with the experimental data to reliably correct the remaining discrepancy with Gaussian Processes, we could still use `CGMF` to evaluate $\overline{\nu}$ but use the standard Los Alamos model [69] to evaluate the PFNS, as has been done for previous evaluations, *e.g.*, in Ref. [4].

Regardless which model code we will use, the following tasks need to be performed for the evaluation next FY:

- Do a more detailed analysis of models and associated parameters within `CGMF` to determine how close we can get with calculated PFNS to experimental data. This task will be lead by A. Lovell with help from T. Kawano, I. Stetcu and P. Talou while teaching D. Neudecker the code. This task includes optimizing the multi-chance fission probabilities and total kinetic energy parametrizations in `CGMF` to reproduce the ENDF/B-VIII.0 evaluation for $\overline{\nu}$. To this end, training a Gaussian Process emulator (as provided by M.J. Grosskopf) would significantly speed up the `CGMF` optimization. This task might take considerable time.

- A decision will need to be taken whether `CGMF` can only be used for $\overline{\nu}$ evaluations or also for PFNS. If `CGMF` cannot be used for PFNS evaluations (even with a Gaussian Process to account for discrepancies compared to experimental data), we will default to the Los Alamos model.

- Model parameter sensitivities and uncertainty values will be determined for `CGMF` by A. Lovell in discussion with D. Neudecker. D. Neudecker will determine the same for the Los Alamos model if we need to default to it.

- D. Neudecker will estimate total covariances for all experimental data deemed reliable for the evaluation using and extending ARIADNE [34] and previous work [4]. She will teach A. Lovell how to do this. Given the volume of data, especially for $\overline{\nu}$, this will be a very time-consuming task.

- A Kalman filter evaluation code including Gaussian Processes will be implemented by A. Lovell and D. Neudecker with guidance from M.J. Grosskopf on the Gaussian Process code he has already written.

- D. Neudecker will perform the evaluation and produce ENDF-6 formatted files including mean values and covariances (MF=5, 35; MT=18 for PFNS and MF=1, 31 MT=456 for $\overline{\nu}$). She will also validate the resulting data with respect to various ICSBEP critical assemblies and LLNL pulsed-sphere neutron leakage spectra.

These results will then be delivered to NCSP. If they prove to be reliable they will also be offered to CSEWG.

Acknowledgments

The authors would like to acknowledge the work of C. Parker, S. Pineda, T. S. Blade, and S. D. Ozier, students from the 2019 and 2020 XCP Computational Physics Workshop, whose hard work over those two summers spurred the optical model potential and Gaussian Process emulation studies shown here. This work was carried out at Los Alamos National Laboratory under the auspices of the NNSA of the U.S. Department of Energy under contract 89233218CNA000001.

References

[1] P. Talou, T. Kawano, I. Stetcu et al. , "Fission Fragment Decay Simulations with the CGMF Code," Comp. Phys. Comm. *in progress.*

[2] B. Becker, P. Talou, T. Kawano et al. , "Monte Carlo Hauser-Feshbach predictions of prompt fission γ rays: Application to $n_{\rm th} + {}^{235}$U, $n_{\rm th} + {}^{239}$Pu, and ^{252}Cf (sf)," Phys. Rev. C **87**, 014617 (2013).

[3] D.A. Brown, M.B. Chadwick, R. Capote et al. , "ENDF/B-VIII.0: The 8th Major Release of the Nuclear Reaction Data Library with CIELO-project Cross Sections, New Standards and Thermal Scattering Data," Nucl. Data Sheets **148**, 1–142 (2018).

[4] D. Neudecker, P. Talou, T. Kawano et al. , "Evaluations of Energy Spectra of Neutrons Emitted Promptly in Neutron-induced Fission of ^{235}U and ^{239}Pu," Nucl. Data Sheets **148**, 293 (2018).

[5] M. Devlin *et al.* , "The Prompt Fission Neutron Spectrum of ^{235}U(n,f) below 2.5 MeV for Incident Neutrons from 0.7 to 20 MeV," Nucl. Data Sheets **148**, 322–337 (2018).

[6] A.C. Wahl, "Systematics of fission-product yields "Los Alamos National Laboratory Report LA-13928 (2002).

[7] A.J. Koning, J.P. Delaroche, "Local and global nucleon optical models from 1 keV to 200 MeV " Nucl. Phys. A **713**, 231–310 (2003).

[8] F.D. Becchetti, G.W. Greenlees, "Nucleon-Nucleus Optical-Model Parameters, $A > 40, E < 50$ MeV " Phys. Rev. **182**, 190 (1969).

[9] R.L. Verner, W.J. Thompson, T.L. McAbee, E.J. Ludwig, T.B. Clegg, "A global nucleon optical model potential " Phys. Rep. **201**, 57–191 (1991).

[10] N. Otuka, E. Dupont, V. Semkova, B. Pritychenko, et al., "Towards a More Complete and Accurate Experimental Nuclear Reaction Data Library (EXFOR): International Collaboration Between Nuclear Reaction Data Centres (NRDC)", Nucl. Data Sheets , **120**, 272–276 (2014). Data available online (*e.g.*, at *www-nds.iaea.org/exfor/*).

[11] D. Neudecker, "Comparing Preliminary Evaluations with Chi-Nu and CEA using the LAM Model for the Prior," Los Alamos National Laboratory Report LA-UR-20-22395 (2020).

[12] D. Neudecker, T.N. Taddeucci, R.C. Haight *et al.* , "The Need for Precise and Well-documented Experimental Data on Prompt Fission Neutron Spectra from Neutron-induced Fission of ^{239}Pu," Nucl. Data Sheets **131**, 289–318 (2016).

[13] R. Capote, Y.-J. Chen, F.-J. Hambsch *et al.* , "Prompt Fission Neutron Spectra of Actinides," Nucl. Data Sheets **131**, 1–106 (2016).

[14] A. S. Vorobyev, O. A. Shcherbakov, "Total prompt fission neutron spectrum from thermal-neutron-induced fission of 235U", Vopr. At. Nauk. Tech., Ser. Yad. Konst., Issue 1-2, 37–54 (2013) [report **INDC(CCP)-0455**, IAEA, Vienna, 2014], EXFOR 41597002.

[15] N. V. Kornilov, F.-J. Hambsch, "Absolute Ratio ^{252}Cf to ^{235}U Prompt Fission Neutron Spectra ", Nucl. Sci. Eng. **168**, 73–74 (2011), EXFOR 31692006.

[16] V. N. Nefedov, B. I. Starostov, A. A. Boytsov, "Precision Measurements of ^{252}Cf, ^{233}U, ^{235}U and ^{239}Pu Prompt Fission Neutron Spectra (PFNS) in the Energy Range 0.04 - 5 MeV", Proc. 6-th All-Union Conf. on Neutron Physics, Kiev, 2-6 Oct. 1983, **Vol. 2**, 285–289 (1983) [report **INDC(CCP)-0457**, IAEA, Vienna, Austria (2014)], EXFOR 40871011, 40871012.

[17] B. I. Starostov, V. N. Nefedov, A. A. Boytsov, "Precision Measurements of ^{252}Cf, ^{233}U+n_{th}, ^{235}U+n_{th} and ^{239}Pu+n_{th} Prompt Fission Neutron Spectra (PFNS) in the Energy Range 2 - 11 MeV", Proc. 6-th All-Union Conf. on Neutron Physics, Kiev, 2–6 Oct. 1983, **Vol. 2**, 290–293 (1983) [report **INDC(CCP)-0458** IAEA, Vienna, Austria (2014)], EXFOR 40872007.

[18] A. A. Boytsov, A. F. Semenov, B. I. Starostov, "Relative Measurements of ^{233}U+n_{th}, ^{235}U+n_{th} and ^{239}Pu+n_{th} Prompt Fission Neutron Spectra (PFNS) in the Energy Range 0.04 – 5 MeV", Proc. 6-th All-Union Conf. on Neutron Physics, Kiev, 2–6 Oct. 1983, **Vol. 2**, 294–297 (1983) [report **INDC(CCP)-0459** IAEA, Vienna, Austria (2014)], EXFOR 40873004.

[19] B. I. Starostov, V. N. Nefedov, A. A. Boytsov, "Prompt Neutron Spectra from Fission of ^{233}U, ^{235}U and ^{239}Pu by Thermal Neutrons and from Spontaneous Fission of ^{252}Cf in the 0.01-12 MeV Energy Range", Vopr. At. Nauk. Tech., Ser. Yad. Konst., **Issue.3**, p.16 (1985) [report **INDC(CCP)-293/L**, p.19 IAEA, Vienna, Austria (1989)], EXFOR 40930.

[20] J. P. Lestone, E. F. Shores, "Uranium and Plutonium Average Prompt-fission Neutron Energy Spectra (PFNS) from the Analysis of NTS NUEX Data", Nucl. Data Sheets **119**, 213–216 (2014).

[21] J. P. Lestone, E. F. Shores, "Uranium and Plutonium Prompt-fission-neutron Spectra (PFNS) of NTS NUEX Data and the Corresponding Uncertainty Budget", LANL report **LA-UR-14-24087**, Los Alamos, USA (2014).

[22] G. S. Boykov, V. D. Dmitriev, G. A. Kudyaev, Yu. B. Ostapenko, M. I. Svirin, G. N. Smirenkin, "Spectrum of Neutrons Accompanying Fission of ^{232}Th,^{235}U, and ^{238}U by 2.9-MeV and 14.7-MeV Neutrons (Below and Above the Threshold of Emission Fission)", Yad. Fiz. **53**, 628–648 (1991) [Sov. J. Nucl. Phys. **53**, 392–406 (1991)], EXFOR 41110.

[23] G. S. Boykov, V. D. Dmitriev, G. A. Kudyaev et al., "Neutron spectrum in the fission of Th-232, U-235, and U-238 by neutrons with energies 2.9 and 14.7 MeV", Phys. Atomic Nucl. **57**, 572 (1994).

[24] B. H. Armitage and M. G. Sowerby (Eds), Proc. EURATOM Specialist Meeting on Inelastic scattering and Fission Neutron Spectra, AERE, Harwell, 14-16 April 1975, Report **AERE-R-8636**, AERE, Harwell, UK (1977). See Appendix A with detailed corrections and numerical data for ^{235}U earlier measurements.

[25] P. I. Johansson, B. Holmqvist, "An Experimental Study of the Prompt Fission Neutron Spectrum Induced by 0.5-MeV Neutrons Incident on ^{235}U", Nucl. Sci. Eng. **62**, 695–708 (1977), EXFOR 20175003. See corrections in Appendix A, AERE-R-8636 (1977) [24].

[26] H.-H. Knitter, M. M. Islam, M. Coppola, "Investigation of Fast Neutron Interaction with U-235 ", Z. Phys. **257**, 108–123 (1972), EXFOR 20394008. See corrections in Appendix A, AERE-R-8636 (1977) [24].

[27] M. M. Islam, H.-H. Knitter, "The Energy Spectrum of Prompt Neutrons from the Fission of Uranium-235 By 0.40-MeV Neutrons", Nucl. Sci. Eng. **50**, 108–114 (1973), EXFOR 20385003. See corrections in Appendix A, AERE-R-8636 (1977) [24].

[28] A. Lajtai, J. Kecskemeti, J. Safar, P. P. Dyachenko, and V. M. Piksaikin, "Energy Spectrum Measurements of Neutrons for Energies 30 keV–4 MeV from Thermal Fission of Main Fuel Elements", NDST 2004, Santa Fe, NM, USA, AIP Conf. Proc. **769**, 613–616 (1985), EXFOR 30704003.

[29] A. Lajtai, P.P. Dyachenko, V.N. Kononov, E.A. Seregina, "Low-Energy Neutron Spectrometer and Its Application for ^{252}Cf Neutron Spectrum Measurements", Nucl. Inst. Meth. Phys. Res. **A293**, 555–561 (1990), EXFOR 41158.

[30] A. Chatillon, G. Baglier, T. Granier, B. Laurent, B. Morillon, J. Taieb, R. C. Haight, M. Devlin, R. O. Nelson, S. Noda, J. M. O'Donnell, "Measurement of prompt neutron spectra from the ^{239}Pu(n,f) fission reaction for incident neutron energies from 1 to 200 MeV", Phys. Rev. **C89**, 014611 (2014), EXFOR 14379.

[31] Th. Granier, "Reanalysis of ^{239} Pu Prompt Fission Neutron Spectra", Phys. Procedia **64**, 183–189 (2015).

[32] H.-H. Knitter, "Measurement of the Energy Spectrum of Prompt Neutrons from the Fission of Pu 239 by 0.215 MeV Neutrons", Atomkernenergie **26**, 76–79 (1975), EXFOR 20576. See corrections in Appendix A, AERE-R-8636 (1977) [24].

[33] P. Marini *et al.* , "Prompt-fission-neutron spectra in the ^{239}Pu(n,f) reaction", Phys. Rev. C **101**, 044614 (2020).

[34] D. Neudecker, "ARIADNE—A Program Estimating Covariances in Detail for Neutron Experiments," Europ. Phys. J. N **4**, 34 (2018).

[35] D. Neudecker, A. Lewis, E. Matthews *et al.*, "Templates of Expected Measurement Uncertainties," Los Alamos National Laboratory Report LA-UR-19-31156 (2019).

[36] V. Ya. Baryba, N. V. Kornilov, O. A. Sal'nikov, Report **947** IPPE, Obninsk, Russia (1979) (in Russian), available in INIS, EXFOR 40740.

[37] B. V. Zhuravlev, L. E. Kazakov, V. J. Kononov, N. V. Kornilov, B. D. Kuz'minov, V. V. Malinovskij, E. D. Poletaev, O. D. Sal'nikov, N. N. Semenova, "Investigations of the Interactions of Neutrons with ^{238}U Nuclei", Report **INDC(CCP)-154/L**, IAEA, Vienna, Austria (1980).

[38] N. V. Kornilov, V. Ja. Baryba, O. A. Sal'nikov, All Union Conf. on Neutron Phys., Kiev, 15–19 Sep 1980 **Vol.3**, 104 (1980) (in Russian), EXFOR 40631.

[39] M. Baba, H. Wakabayashi, M. Ishikawa, N. Nakashima, N. Ito, N. Hirakawa, "Fission Spectrum Measurement of ^{232}Th and ^{238}U for 2 MeV Neutrons", pp.149–159, EXFOR 22112.

[40] G. S. Boykov et al., "New Data on Prefission Neutrons", Z. Phys. **A340**, 79–84 (1991).

[41] G. N. Smirenkin, G. N. Lovchikova, A. M. Trufanov, M. I. Svirin, A. V. Polyakov, V. A. Vinogradov, V. D. Dmitriev, G. S. Boykov, "Measurement of Energy Spectrum of Neutrons Accompanying Emission Fission of U-238 nuclei", Yad. Fiz. **59**, 1934–1939 (1996) [Phys. At. Nuclei **59**, 1865–1870 (1996)], EXFOR 41461.

[42] A. M. Trufanov, G. N. Lovchikova, M. I. Svirin, A. V. Polyakov, V. A. Vinogradov, V. D. Dmitriev, G. S. Boykov, "Investigation of the Spectra of Neutrons Originating from ^{238}U Fission Induced by 5.0- and 13.2-MeV Neutrons", Yad. Fiz. **64**, 3–10 (2001) [Phys. At. Nuclei **64**, 1–8 (2001)], EXFOR 41450.

[43] G. N. Lovchikova, A. M. Trufanov, M. I. Svirin, V. A. Vinogradov, A. V. Polyakov , "Spectra and Mean Energies of Prompt Neutrons from ^{238}U Fission Induced by Primary Neutrons of Energy in the Region $E_n < 20$ MeV", Yad. Fiz. **67**, 1270–1287 (2004) [Phys. At. Nuclei **67**, 1246–1263 (2004)], EXFOR 41447.

[44] V. V. Desai, B. K. Nayak, A. Saxena, S. V. Suryanarayana, R. Capote, "Prompt fission neutron spectra in fast neutron induced fission of ^{238}U", Phys. Rev. **C92** 014609 (2015).

[45] J.W. Boldeman and M.G. Hines, "Prompt Neutron Emission Probabilities Following Spontaneous and Thermal Neutron Fission," Nucl. Sci. Eng. **91**, 114–116 (1985); J.W. Boldeman and R.L. Walsh, "The Energy Dependence of $\overline{\nu}_p$ for Neutron Induced Fission of ^{235}U below 2.0 MeV," J. Nucl. Energy **24**, 191–205 (1970).

[46] H. Condé, J. Hansén and M. Holmberg, "Prompt $\overline{\nu}_{\rm tot}$ in Neutron-induced Fission of ^{239}Pu and ^{241}Pu, " J. of Nucl. Energy **22**, 53–60 (1968).

[47] B.C. Diven, H.C. Martin, R.F. Taschek, "Multiplicities of Fission Neutrons," Phys. Rev. **101** 1012–1016 (1956).

[48] M. Soleihac, J. Frehaut and J. Gauriau, "Energy Dependence of $\overline{\nu}_p$ for Neutron-induced Fission of ^{235}U, ^{238}U and ^{239}Pu from 1.3 to 15 MeV," J. of Nucl. Energy **23**, 257–282 (1969); J. Frehaut, G. Mosinski and M. Soleihac, "Recent Results in $\overline{\nu}_p$ Measurements between 1.5 and 15 MeV," Topical Conference on $\overline{\nu}_p$ The Average Number of Neutrons Emitted in Fission, France, 1972, Report EANDC(E)-15 "U" (1973).

[49] R. Gwin, R.R. Spencer and R.W. Ingle, "Measurements of the Energy Dependence of Prompt Neutron Emission from ^{233}U, ^{235}U, and ^{239}Pu for E_n =0.0005 to 10 MeV Relative to Emission from Spontaneous Fission of ^{252}Cf," Nucl. Sci. Eng. **94**, 365–379 (1986); R. Gwin, R.R. Spencer and R.W. Ingle,"Measurements of the Energy Dependence of Prompt Neutron Neutron Emission from ^{233}U, ^{235}U, ^{239}Pu, and ^{241}Pu for E_n =0.0005 to 10 eV Relative to Emission from Spontaneous Fission of ^{252}Cf," Nucl. Sci. Eng. **87**, 381–404 (1984); R. Gwin, R.R. Spencer, R.W. Ingle et al. ,"Measurements of the Average Number of Prompt Neutrons Emitted per Fission of ^{239}Pu and ^{235}U," Oak Ridge National Laboratory ORNL/TM-6246 (1978).

[50] J.C. Hopkins and B.C. Diven, "Prompt neutrons from fission," Nuclear Physics, **48**, 433 (1963).

[51] Z. Huanqiao, X. Jincheng, L. Zuhua et al. , "The Dependence of Average Numbers of Prompt Fission Neutron of Pu-239 on Incident Fast Neutron Energies," Chin. J. of Nucl. Phys. **2**, 29 (1980).

[52] I. Johnstone, "A Measurement of the Average Number of Prompt Neutrons Emitted in Fission at High Energy,"Atomic Energy Research Establishment Report A.E.R.E NP/R 1912 (1956).

[53] V.I. Kalashnikova, V.I. Lebedev, P.E. Spivak et al. , "Absolute Evaluation of the Average Number of Neutrons Emitted in the Fission of some Isotopes of Uranium and Plutonium," Proc. of the USSR Conf. peaceful Uses of Atomic Energy, USSR 1955, 156 (1955).

[54] M.V. Savin, Yu.A. Khokhlov, A.E. Savelév et al. , "Energy Dependence of $\overline{\nu}_{\rm tot}$ in the Fission of U^{235} by Fast Neutrons," Soviet J. of Nucl. Physics **16**, 638–640 (1973).

[55] P.J. Leroy, "Nombres Moyens de Neutrons Prompts Èmis Dans La Fission de ^{238}U, ^{239}Pu, ^{232}Th," Le Journal de Physique et le Radium **21**, 617–628 (1960).

[56] D.S. Mather, P. Fieldhouse and A. Moat, "Measurement of Prompt $\overline{\nu}_{\rm tot}$ for the Neutron-induced Fission of Th^{233}, U^{233}, U^{234}, U^{238} and Pu^{239}," Nucl. Phys. A **66**, 149–160 (1965).

[57] L.I. Prokhorova, R.E. Bagdasarov, I.I. Kotukhov et al. , "Yield of Prompt Neutrons $\overline{\nu}_{\rm tot}$ in the Fission of U^{235} by Neutrons with Energies up to 1.5 MeV," Atomnaya Énergiya **30**, 250–257 (1971).

[58] B. Nurpeisov, K.E. Volodin, V.G. Nesterov et al. , "Dependence of $\overline{\nu}_{\rm tot}$ on Neutron Energies up to 5 MeV for ^{233}U, U^{235}, and ^{239}Pu," Atomnaya Énergiya **39**, 199–205 (1975).

[59] M.V. Savin,Yu.A. Khokhlov,Yu.S. Zamjatnin et al. , "The Average Number of Prompt Neutrons in Fast Neutron Induced Fission of U-235, Pu-239 and Pu-240," IAEA Report IAEA-CN-26/40 (1970).

[60] G.N. Smirenkin, I.I. Bondarenko, L.S. Kutsaeva et al. , "Mean Number of Prompt Neutrons in the Fission of U^{233}, U^{235}, Pu^{239} by 4 and 15 MeV Neutrons," Sov. Atomic Energy **4**, 253–255 (1958).

[61] M. Soleihac, J. Fréhaut, J. Gauriau et al. , "Average Number of Prompt Neutrons and Relative Fission Cross-Sections of U-235 and Pu-239 in the 0.3 to 1.4 MeV Range," Proc. of the Conference for Nuclear Data for Reactors, Helsinki, **2**, 145– (1970); J.W. Boldeman, J. Fréhaut and R.L. Walsh, "A Reconciliation of Measurements of $\overline{\nu}_p$ for Neutron-induced Fission of Uranium-235," Nucl. Sci. Eng. **63**, 430–436 (1977).

[62] K.E. Bolodin, V.F. Kuznetsov, V.G. Nesterov et al. , "Average Number of Prompt Neutrons in Pu^{239} Fission," Atomnaya Énergiya **33**, 901–906 (1972).

[63] R.L. Walsh and J.W. Boldeman, "The Energy Dependence of $\overline{\nu}_p$ for ^{233}U, ^{235}U and ^{239}Pu below 5.0 MeV," J. Nucl. Energy **25**, 321–330 (1971).

[64] S. Okumura, T. Kawano, P. Jaffke, P. Talou, S. Chiba, "^{235}U(n, f) Independent fission product yield and isomeric ratio calculated with the statistical Hauser-Feshbach theory " J. Nuc. Sci. Tech. **55**, 1009–1023 (2018).

[65] D. Neudecker et al. , "Validating Nuclear Data Uncertainties Obtained from a Statistical Analysis of Experimental Data with the "Physical Uncertainty Bounds" Method," EPJ Nuclear Sci. Technol. **6**, 19 (2020).

[66] D.E. Vaughan and D.L. Preston, "Physical Uncertainty Bounds (PUB)," Los Alamos National Laboratory Report LA-UR-14-20441.

[67] I. Stetcu, P. Talou, T. Kawano, M. Jandel, "Properties of prompt fission γ rays " PHYS. REV. C **90**, 024617 (2014).

[68] R. Capote, M. Herman, P. Obložinský et al. , "RIPL—Reference Input Parameter Library for Calculation of Nuclear Reactions and Nuclear Data Evaluations," NUCL. DATA SHEETS **110**, 3107–3214 (2009).

[69] D.G. Madland and J.R. Nix, "New Calculation of Prompt Fission Neutron Spectra and Average Prompt Neutron Multiplicities," NUCL. SCI. ENG. **81**, 213–271 (1982).

[70] C.E. Rasmussen, C.K.I. Williams, "Gaussian Processes for Machine Learning ", the MIT Press (2006).